

# Probing Massive Stars around Gamma-Ray Burst Progenitors

Wenbin Lu,<sup>1\*</sup> Pawan Kumar,<sup>1†</sup> George F. Smoot<sup>2‡</sup>

<sup>1</sup>*Department of Astronomy, University of Texas at Austin, Austin, TX 78712, USA*

<sup>2</sup>*PCCP; APC, Université Paris Diderot, Université Sorbonne Paris Cité, 75013 Paris, France*

<sup>2</sup>*BCCP; LBNL & Physics Dept. University of California at Berkeley CA 94720, USA*

6 August 2021

## ABSTRACT

Long Gamma-Ray Bursts (GRBs) are produced by ultra-relativistic jets launched from core collapse of massive stars. Most massive stars form in binaries and/or in star clusters, which means that there may be a significant external photon field (EPF) around the GRB progenitor. We calculate the inverse-Compton scattering of EPF by the hot electrons in the GRB jet. Three possible cases of EPF are considered: the progenitor is (*I*) in a massive binary system, (*II*) surrounded by a Wolf-Rayet-star wind, and (*III*) in a dense star cluster. Typical luminosities of  $10^{46} - 10^{50}$  erg/s in the 1 - 100 GeV band are expected, depending on the stellar luminosity, binary separation (*I*), wind mass loss rate (*II*), stellar number density (*III*), etc. We calculate the lightcurve and spectrum in each case, taking fully into account the equal-arrival time surfaces and possible pair-production absorption with the prompt  $\gamma$ -rays. Observations can put constraints on the existence of such EPFs (and hence on the nature of GRB progenitors) and on the radius where the jet internal dissipation process accelerates electrons.

**Key words:** radiation mechanisms: non-thermal - methods: analytical - gamma-ray burst: general.

## 1 INTRODUCTION

Long Gamma-Ray Bursts (GRBs) are produced by ultra-relativistic jets launched after the collapse of massive stars (e.g. Galama et al. 1998; Hjorth et al. 2003; Piran 2004; Woosley & Bloom 2006). Massive stars tend to form in binaries and/or in dense star clusters (Massey & Hunter 1998; Zinnecker & Yorke 2007; Mason et al. 2009; Portegies Zwart et al. 2010), which produce a dense external photon field (EPF) around the GRB progenitor. Soft photons will be inverse-Compton (IC) scattered by electrons in the jet. The scattering will boost the energy of photons by a factor of  $\Gamma^2 \gamma_e^2$ , where  $\Gamma \sim 300$  is the jet bulk Lorentz factor (LF) and  $\gamma_e$  is electrons' LF in the comoving frame. Therefore, we expect EPF at 10 eV being scattered to  $10^6 \gamma_e^2$  eV.

In the GRB literature, this external inverse-Compton (EIC) emission has been considered for a variety of sources of soft photons and scattering electrons. For example, the soft photons may come from a pulsar wind bubble created

before the GRB (Guetta & Granot 2003), and from the funnel of the collapsing star created during the jet breakout (Lazzati et al. 2000; Ghisellini et al. 2000; MacFadyen et al. 2001). Ramirez-Ruiz (2004) considered soft photons from a companion star being IC scattered by a magnetically driven relativistic wind from a spinning-down millisecond supramagnetar. Giannios (2008); Mimica & Giannios (2011) considered the GRB external shock interacting with the photon field from an O star in the surrounding dense cluster.

Different from previous studies, we consider three cases where significant EPFs exist: the GRB progenitor (*I*) is in a massive binary system, (*II*) has a strong wind, and (*III*) is in a dense star cluster.

In *Case I*), soft photons come from a massive companion star. Spectroscopic and direct imaging studies of Galactic massive stars, although biased by selection effects and measurement limitations, conclude that massive stars have binary fraction of at least  $\sim 50\%$  (see Mason et al. 2009, and reference therein). Therefore, a companion of comparable mass may exist near the GRB progenitor, depending on the evolution status of the binary system (Langer 2012). For binary separation  $d = 10^{15}$  cm and the companion star's bolometric luminosity  $L_b = 10^{39}$  erg/s, the number of scattered photons will be  $10^{52} - 10^{53}$  (isotropic equivalent).

\* wenbinlu@astro.as.utexas.edu

† pk@astro.as.utexas.edu

‡ gfsmoot@lbl.gov

In *Case (II)*, soft photons originally from the progenitor star are scattered first by the electrons in the stellar wind and again by the jet. A compact Wolf-Rayet (W-R) star progenitor is favored by considering the propagation time of a GRB jet in the stellar envelope (Matzner 2003). W-R stars have high luminosities of  $\sim 10^{39}$  erg/s and are surrounded by strong stellar wind of a typical mass loss rate  $10^{-5} M_{\odot}/\text{yr}$  (Crowther 2007). The number of scattered photons is  $10^{50} - 10^{51}$  (isotropic equivalent).

In *Case (III)*, all the stars in the cluster create a nearly isotropic and uniform EPF around the GRB jet. Massive stars form in clustered environments (Lada & Lada 2003). In our Galaxy,  $\sim 85\%$  of O stars are either observed in young clusters or directly identified as runaways (see Portegies Zwart et al. 2010, and reference therein). Within the central  $\sim 0.2$  pc of Arches Cluster, the densest known young massive cluster in the Milky Way, the number density of massive ( $30 < M/M_{\odot} < 120$ ) stars is  $\sim 5000$  pc $^{-3}$  (Espinoza et al. 2009). These stars have luminosities close to or higher than  $10^{39}$  erg/s. Long GRBs are associated with actively star-forming galaxies (Fruchter et al. 2006; Woosley & Bloom 2006), where young massive clusters are particularly abundant (Portegies Zwart et al. 2010). Therefore, we expect a good fraction, depending on the clusters' evolution, of long GRBs to happen in such star clusters. In this *Case*, we consider EIC emission from both internal dissipation and external shocks (both reverse shock and forward shock). Note that our model is different from Giannios (2008), who consider the case when the external forward shock happens to sweep across one star in the cluster. Mimica & Giannios (2011) also calculate the EIC scattering of the isotropic diffuse EPF in the cluster, but only the external forward shock is considered. As shown in Section 3.1.3, the EIC luminosity is dominated by the internal dissipation and reverse shock.

In this paper, we show that all three cases may have observable consequences, which can be used to probe massive stars around GRB progenitors and the nature of GRB progenitors.

A few more notes. (1) By “internal dissipation” (ID) we mean the uncertain process (e.g. internal shock or magnetic reconnection, see Kumar & Zhang 2015, for a recent review) that dissipates the free energy of the jet and produces the prompt  $\gamma$ -rays. As long as electrons are accelerated to an ultra-relativistic powerlaw, our model is independent of the details of the jet dissipation and particle acceleration process. (2) The opening angle of the jet is assumed to be larger than the causally connected cone, i.e.  $\theta_{j,max} > 1/\Gamma$ , so we use the isotropic equivalent energy, luminosity, photon number, etc throughout the paper. (3) The jet is assumed to be hadron dominated and made of pure protons and electrons<sup>1</sup>. (4) The convention  $X_n = X/10^n$  in CGS units is adopted.

This paper is organized as follows. In Section 2, we

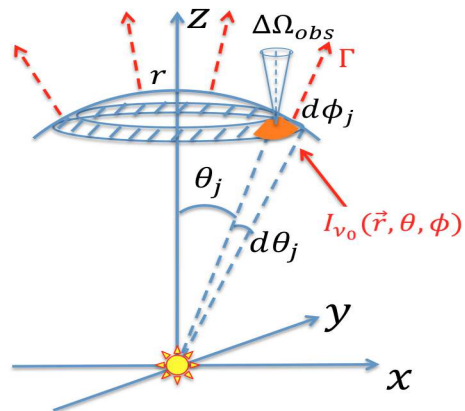


**Figure 1.** Lab frame (progenitor’s rest frame). A spherically capped jet is moving in the  $z$  direction with bulk Lorentz factor  $\Gamma$ . We consider a small volume element (orange)  $r^2 d\Omega_j dr = r^2 \sin\theta_j d\theta_j d\phi_j dr$  of the jet at position  $\vec{r} = (r, \theta_j, \phi_j)$ . The external photon field at position  $\vec{r}$  is denoted by intensity  $I_{\nu_0}(\vec{r}, \theta, \phi)$ , where  $(\theta, \phi)$  is photons’ moving direction. Photons scattered into the observer’s cone  $\Delta\Omega_{obs}$  are considered as observed.

give a general treatment of the EIC emission (spectrum and lightcurve) when a jet interacts with an arbitrary EPF. In Section 3, we first give simple order-of-magnitude estimates of the total EIC energy in the three cases, and then put the specific EPFs into the general procedures and calculate the precise lightcurves and spectra. In Section 4, we discuss some potential issues, e.g. absorption of high energy  $\gamma$ -rays by the cosmic background light or by the local EPF itself. Short conclusion is given in Section 5.

## 2 MODELING THE EIC EMISSION

In this section, we provide a general calculation for the lightcurve and spectrum expected for an observer on the jet axis, when a relativistic jet makes its way through an arbitrary external photon field (EPF).

EIC emission has been studied extensively in the literature, for instance in active galactic nuclei (e.g. Dermer & Schlickeiser 1993) where a jet meets an EPF. We refer the readers to Blumenthal & Gould (1970); Aharonian & Atoyan (1981) for a general treatment on IC radiation. Also, Fan et al. (2008) give a review of IC radiation in GRB afterglows, including EIC and synchrotron-self Compton (SSC) radiation. Our treatment is different only in that, at an early stage, equal-arrival time surfaces are taken into consideration. Experienced readers could skip Section 2 and go to Section 3 for the results.

In terms of notations, (1) we use un-primed quantities in the lab frame (rest frame of the progenitor star) and primed ( $'$ ) ones in the jet comoving frame, and quantities with subscript “ $j$ ”, e.g.  $(\theta_j, \phi_j)$ , are related to different regions in the jet. Note that, by “comoving frame” we mean “comoving” with the bulk motion of the jet, rather than the host galaxy’s redshift. (2) We denote the unscattered and scattered photons’ frequencies as  $\nu_0$  ( $\nu'_0$ ) and  $\nu$  ( $\nu'$ ) in the lab (comoving) frame.

As shown in Fig.(1), the jet is moving with a Lorentz factor (LF)  $\Gamma$  in the  $z$  direction at radius  $r$ . For a volume

<sup>1</sup> Hadrons carry the momentum of the jet but are neglected in the IC scattering process (since there is an equal amount of electrons). If the jet is magnetically dominated, we expect the EIC emission from the internal dissipation to be much weaker, due to a much smaller number of electrons. For a multi-element jet, e.g. Hydrogen and Helium, our model can be easily modified by putting a  $(1 + X(H))/2$  factor before  $E_j$  (the total kinetic energy of the jet), where  $X(H)$  is the mass fraction of Hydrogen.

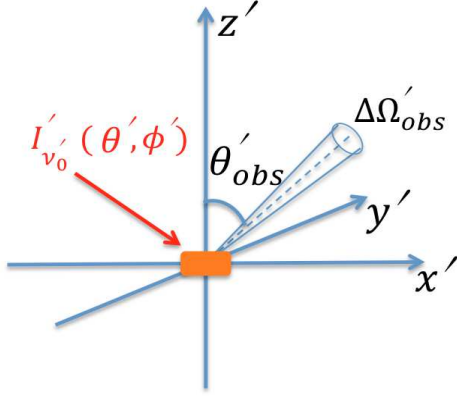


**Figure 2.** Comoving frame of the volume element (orange) in Fig.(1). External photon field is denoted by intensity  $I'_{\nu_0}(\theta', \phi')$ . The observer's cone  $\Delta\Omega'_{obs}$  is in the  $x'z'$  plane. Photons scattered into  $\Delta\Omega'_{obs}$  are considered as observed.

element (orange) at position  $\vec{r} = (r, \theta_j, \phi_j)$ , our goal is to consider all the EPF that is scattered into the observer's cone  $\Delta\Omega_{obs}$ , which is a very small solid angle in the  $z$  direction considering the cosmological distances<sup>2</sup>. The EPF specific intensity is denoted as  $I_{\nu_0}(\vec{r}, \theta, \phi)$ , where  $\vec{r}$  is the position of the volume element and  $(\theta, \phi)$  is the direction in which photons are moving.

In the comoving frame of the volume element, the observer's cone is

$$\Delta\Omega'_{obs} = D_j^2 \Delta\Omega_{obs} \quad (1)$$

where  $D_j$  is the Doppler factor

$$D_j = \frac{1}{\Gamma(1 - \beta \cos\theta_j)} \quad (2)$$

and  $\beta = \sqrt{1 - 1/\Gamma^2}$  is the velocity of the jet.

Fig.(2) shows the geometry in the comoving frame, where  $z'$  axis is aligned with the original moving direction of the volume element. We orient the  $x'$  axis in a way that the observer's cone is in the  $x'z'$  plane and at an angle  $\theta'_{obs}$  with the  $z'$  axis. Recall that in the lab frame,  $\theta_j$  is the angle between observer's cone (same as  $z$  axis) and the moving direction of the volume element. Therefore, Lorentz transformation (LT) gives

$$\cos\theta'_{obs} = \frac{\cos\theta_j - \beta}{1 - \beta \cos\theta_j} \quad (3)$$

Going from  $I_{\nu_0}(\theta, \phi)$  to  $I'_{\nu_0}(\theta', \phi')$  needs an axis rotation and a LT. The axis rotation from  $xyz$  frame to  $\hat{x}\hat{y}\hat{z}$  frame, in which  $\hat{z}$  axis points towards the moving direction, can be expressed by

$$(\vec{e}_1, \vec{e}_2, \vec{e}_3) = R_{\hat{y}}(\theta_j) R_{\hat{z}}(\pi - \phi_j) (\vec{e}_1, \vec{e}_2, \vec{e}_3) \quad (4)$$

where  $\{\vec{e}_i\}$  and  $\{\hat{e}_i\}$  ( $i = 1, 2, 3$ ) are respectively the basis vectors in the  $xyz$  and  $\hat{x}\hat{y}\hat{z}$  frame.  $R_{\hat{y}, \hat{z}}(\alpha)$  are rotation operators, along  $\hat{y}$  or  $\hat{z}$  axis by an angle  $\alpha$  according to the

<sup>2</sup> When calculating the isotropic equivalent luminosity, we use  $\Delta\Omega_{obs} = 4\pi$ . Throughout this paper, if not specially stated, luminosities, emission energies, frequencies and observer's time are presented in the host galaxy frame.

right-hand rule. Therefore, a one-to-one map  $(\theta, \phi) \rightarrow (\tilde{\theta}, \tilde{\phi})$  is obtained from Eq.(4). Then LT gives the intensity in the comoving frame

$$I'_{\nu_0}(\theta', \phi') = \tilde{I}_{\nu_0}(\tilde{\theta}, \tilde{\phi}) \cdot \left(\frac{\nu'_0}{\nu_0}\right)^3 \quad (5)$$

and frequency

$$\nu_0 = \Gamma(1 + \beta \cos\theta') \nu'_0 \quad (6)$$

and direction

$$\cos\tilde{\theta} = \frac{\cos\theta' + \beta}{1 + \beta \cos\theta'}, \quad \tilde{\phi} = \phi' \quad (7)$$

In the comoving ( $x'y'z'$ ) frame, if electrons are assumed to be moving isotropically with LF  $\gamma_e$ , the (average) differential IC cross section from  $(\nu'_0, \theta', \phi')$  to  $(\nu', \theta'_{obs}, \phi'_{obs} = 0)$  is<sup>3</sup> (Aharonian & Atoyan 1981)

$$\frac{\partial^2 \sigma}{\partial \nu' \partial \Omega'_{obs}} \simeq \frac{3\sigma_T}{16\pi\gamma_e^2 \nu'_0} \left[ 1 + \frac{z^2}{2(1-z)} - \frac{2z}{b_\theta(1-z)} + \frac{2z^2}{b_\theta^2(1-z)^2} \right] \quad (8)$$

where  $z = h\nu'/(\gamma_e m_e c^2)$ ,  $b_\theta = 2(1 - \cos\theta'_{ic})\gamma_e h\nu'_0/(m_e c^2)$ ,  $h\nu'_0 \ll h\nu' \leq \gamma_e m_e c^2 b_\theta/(1 + b_\theta)$ ,  $\theta'_{ic}$  is the angle between the direction of incident and scattered photons, i.e.  $\cos\theta'_{ic} = \sin\theta'_{obs} \cos\phi' \sin\theta' + \cos\theta'_{obs} \cos\theta'$ ,  $m_e$  is electron mass,  $c$  is speed of light, and  $\sigma_T$  is Thomson cross section.

We consider a powerlaw distribution of electrons

$$dn_e \begin{cases} \propto \gamma_e^{-p} d\gamma_e & \text{if } \gamma_e \geq \gamma_m \\ = 0 & \text{otherwise} \end{cases} \quad (9)$$

Therefore, the averaged differential cross section becomes

$$\begin{aligned} \left\langle \frac{\partial^2 \sigma}{\partial \nu' \partial \Omega'_{obs}} \right\rangle_{\gamma_e} &= \frac{\int_{\gamma_m}^{\infty} \frac{\partial^2 \sigma}{\partial \nu' \partial \Omega'_{obs}} \gamma_e^{-p} d\gamma_e}{\int_{\gamma_m}^{\infty} \gamma_e^{-p} d\gamma_e} \\ &= (p-1) \left( \frac{\gamma_m m_e c^2}{h\nu'} \right)^{p+1} \frac{3\sigma_T}{16\pi\gamma_m^2 \nu'_0} \\ &\cdot \int_0^{z_{max}} \left[ 1 + \left( \frac{1}{2} - \frac{2}{a_\theta} \right) \frac{z^2}{1-z} + \frac{2}{a_\theta^2} \frac{z^4}{(1-z)^2} \right] z^p dz \end{aligned} \quad (10)$$

where  $a_\theta = 2(1 - \cos\theta'_{ic})h^2\nu'_0\nu'/(m_e c^2)^2$ ,  $z_{max} = \min(h\nu'/(\gamma_m m_e c^2), (\sqrt{a_\theta^2 + 4a_\theta} - a_\theta)/2)$ . Note that  $a_\theta \simeq h^2\nu'_0\nu'/(m_e c^2)^2$  is roughly the criterion for whether EIC scattering is in the Klein-Nishina (KN) regime.

In the low energy band  $\nu'/(\gamma_m^2\nu'_0) < 1$ , the differential cross section  $\propto \nu'^0$  (i.e. constant), so we expect  $\nu' L_{\nu'} \propto \nu'^2$ . In the high energy band  $\nu'/(\gamma_m^2\nu'_0) > 1$ , we have

$$\begin{aligned} z_{max} &= \left( \sqrt{a_\theta^2 + 4a_\theta} - a_\theta \right) / 2 \\ &= \begin{cases} 1 - 1/a_\theta + O(1/a_\theta^2) & \text{if } a_\theta \gg 1 \\ \sqrt{a_\theta} + O(a_\theta) & \text{if } a_\theta \ll 1 \end{cases} \end{aligned} \quad (11)$$

Then we get

$$\left\langle \frac{\partial^2 \sigma}{\partial \nu' \partial \Omega'_{obs}} \right\rangle_{\gamma_e} \propto \begin{cases} \nu'^{-(p+1)/2} & \text{if } a_\theta \ll 1 \\ \nu'^{-(p+1)} (\ln(a_\theta) + C) & \text{if } a_\theta \gg 1 \end{cases} \quad (12)$$

as pointed out by Blumenthal & Gould (1970) and Aharonian & Atoyan (1981). Therefore, in the Thomson

<sup>3</sup> The approximation is good if  $\gamma_e \gg 1$ .

regime ( $a_\theta \ll 1$ ), we expect  $\nu' L_{\nu'} \propto \nu'^{(3-p)/2}$ ; in the KN regime ( $a_\theta \gg 1$ ), we expect  $\nu' L_{\nu'} \propto \nu'^{1-p}$ . However, as we shall see in Section 3.2, the EIC spectrum is almost never  $\nu'^{(3-p)/2}$  or  $\nu'^{1-p}$ . The reasons are as follows: (1) When  $\nu/(\Gamma^2 \gamma_m^2 \nu_0) < 1$ , we are generally in the Thomson regime, and hence we get  $\nu L_\nu \propto \nu^2$ . (2) When  $\nu/(\Gamma^2 \gamma_m^2 \nu_0) > 1$ , we almost immediately get into the KN regime ( $a_\theta > 1$ ), and the  $(\ln(a_\theta) + C)$  factor can't be ignored until  $a_\theta \geq 100$  (i.e.  $h\nu \geq 3 \text{ TeV}$ ). As the high energy tail suffers from pair-production absorption (see the Appendix), the spectra hardly reach  $\text{TeV}$  band.

Suppose the volume element (orange in Fig.1) contains  $dN_e$  electrons, the number of photons that are scattered into  $d\Omega'_{obs}$ , in a time duration  $dt'$  and frequency range  $d\nu'$ , is

$$dN_\gamma = dN_e \cdot d\nu' \Delta\Omega'_{obs} dt' \cdot \int_{4\pi} d\Omega' \int_0^\infty d\nu'_0 \frac{I'_{\nu'_0}(\theta', \phi')}{h\nu'_0} \left\langle \frac{\partial^2 \sigma}{\partial \nu' \partial \Omega'_{obs}} \right\rangle_{\gamma_e} e^{-\tau(\nu'_0, \theta')} \quad (13)$$

where the optical depth  $\tau(\nu'_0, \theta')$  describes the attenuation by the part of the jet that lies along the incident photons' trajectory before they enter the jet volume element where the IC scattering is considered. Second scattering is ignored here. We assume the jet is launched steadily with (isotropic) power  $L_j$  and duration  $T_j$ , total (isotropic) kinetic energy is  $E_j$ , and the thickness of the jet is  $\Delta r = cT_j$ . Photons are all assumed to enter the jet from the front surface, which is at radius  $r$ . If the volume element is located  $\delta r$  from the jet front, the optical depth along the incident photons' trajectory is

$$\tau(\nu'_0, \theta') = \frac{\delta r}{\Delta r} \frac{E_j}{\Gamma m_p c^2} \sigma_{tot}(\nu'_0) \cdot \frac{1}{4\pi r^2 |\cos\theta'|} \quad (14)$$

where  $|\cos\theta'|$  is due to the incident angle onto the front surface and  $\sigma_{tot}(\nu'_0)$  is the total KN cross section averaged over electrons' powerlaw distribution

$$\sigma_{tot}(\nu'_0) = \frac{\int_{\gamma_m}^\infty \sigma_{KN}(\nu'_0, \gamma_e) \gamma_e^{-p} d\gamma_e}{\int_{\gamma_m}^\infty \gamma_e^{-p} d\gamma_e} \quad (15)$$

Actually, not all the  $dN_\gamma$  (Eq.13) photons will be observed. Photons of energy  $h\nu \gtrsim 10 \text{ GeV}$  may collide with low energy photons (such as the GRB prompt emission) and produce pairs. In the Appendix, we calculate the pair-production optical depth  $\tau_{\gamma\gamma}(\nu, r)$  (Eq.A9) for high energy photons produced at radius  $r$  and have frequency  $\nu$ . Basically, we show that only the absorption by the GRB prompt emission may be important, if the prompt emission is produced at the same radius. And we use a broken powerlaw spectrum (Band et al. 1993) with low (high) frequency index  $-1$  ( $-2.4$ ), break frequency  $200 \text{ keV}$  and bolometric isotropic luminosity  $10^{52} \text{ erg/s}$ , following the *Fermi* GRB statistics (Gruber et al. 2014). Then, the  $dN_\gamma$  in Eq.(13) needs to be multiplied by  $e^{-\tau_{\gamma\gamma}}$ .

Next we include the effect of the conical shape of the jet ("curvature effect") on the observed luminosity. When the jet front is at radius  $r$ , the scattered photons from a volume element at a distance  $\delta r$  from the jet front and at latitude  $\theta_j$  will arrive at observer's time  $t_{obs}(r, \delta r, \theta_j)$ . Photons arriving at the same time are from the same equal-arrival time surface, described by

$$r_{eq}(\theta_j, \delta r, t_{obs}) = \beta \frac{ct_{obs} - \delta r}{1 - \beta \cos\theta_j} \quad (16)$$

We divide the jet into many thin shells of thickness  $d(\delta r)$  according to the distance to the jet front  $\delta r$  and calculate the lightcurve contributed by each shell. Using Lorentz transformation in time  $dt' = dr_{eq}/(\Gamma c) \simeq D_j dt_{obs}$  and frequency  $\nu' = \nu/D_j$  in Eq.(13), we obtain the specific luminosity from one shell  $d(\delta r)$  at  $\delta r$

$$dL_\nu = \frac{dN_\gamma h\nu}{d\nu dt_{obs}} e^{-\tau_{\gamma\gamma}(\nu, r)} = \frac{E_j}{\Gamma m_p c^2} \frac{d(\delta r)}{\Delta r} \frac{\int d\Omega_j}{4\pi} h\nu D_j^2 \Delta\Omega_{obs} e^{-\tau_{\gamma\gamma}(\nu, r)} \cdot \int_{4\pi} d\Omega' \int_0^\infty d\nu'_0 \frac{I'_{\nu'_0}(\theta', \phi')}{h\nu'_0} \left\langle \frac{\partial^2 \sigma}{\partial \nu' \partial \Omega'_{obs}} \right\rangle_{\gamma_e} e^{-\tau(\theta')} \quad (17)$$

where  $\int d\Omega_j = \int_0^{\theta_{j,max}} \sin\theta_j d\theta_j \int_0^{2\pi} d\phi_j$  and we use  $\theta_{j,max} = 4/\Gamma$  (not sensitive) in our numerical results (Section 3.2). Then, the total observed luminosity is obtained by adding up all the shells, i.e. integrating Eq.(17) over  $\int_0^{\Delta r} d(\delta r)$ .

### 3 APPLICATIONS

In this section, we apply the procedures developed in Section 2 to three different cases, where the EPFs are given by the physical environment. First, in Section 3.1, we give simple order-of-magnitude estimates of the total EIC energy, not considering the pair production. See Table (1) for the summary of our estimates on peak frequency, EIC luminosity, duration, etc in all cases. Then in Section 3.2, we present the EIC lightcurves and spectra, with absorption from pair production (with prompt  $\gamma$ -rays) considered. For simplicity, each case is considered separately in this paper, but in reality, different cases can operate simultaneously (e.g. the GRB progenitor is in a binary system and has a wind) and the total EIC emission will approximately be a superposition of them.

#### 3.1 Order-of-magnitude Estimate

##### 3.1.1 Case (I) — Binary System

Consider the GRB progenitor star being in a binary system. Soft photons from the companion star are scattered by the electrons in the relativistic jet.

We assume the direction of the jet is perpendicular to the orbital plane<sup>4</sup>. As shown in Fig.(3), the jet is at a distance  $r$  from the progenitor star (A) and is moving with LF  $\Gamma$  in the  $z$  direction, and the companion star (B) is on the  $x$  axis at a distance  $d$  from A. Photons from Star B encounter the jet at an angle  $\cos\theta_* = r/\sqrt{r^2 + d^2}$ .

Suppose the companion star has a bolometric luminosity  $L_b = 10^{39} \text{ erg/s}$   $L_{b,39}$  and peak energy  $\epsilon_0 = 10 \text{ eV}$   $\epsilon_{0,1}$ . Considering the possible recoil of electrons, we estimate the energy of scattered photons by

$$\epsilon \simeq \min(\Gamma^2 \gamma_e^2 \epsilon_0, \Gamma \gamma_e m_e c^2) = 9 \text{ GeV} \Gamma_{2.5}^2 \gamma_{e,2}^2 \epsilon_{0,1} \eta_{KN} \quad (18)$$

<sup>4</sup> Even if the jet direction is inclined by up to  $30^\circ$  from the normal direction of orbital plane, the total energy (or luminosity) will be affected by a factor of order unity ( $\lesssim 2$ ).

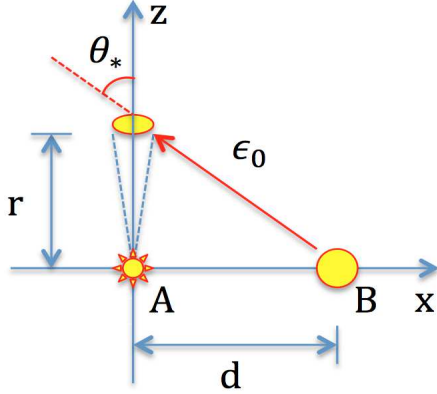


**Figure 3.** Geometry of Case (I). The jet is on the z axis at a distance  $r$  from the progenitor star (A). The companion star (B) is on the x axis at a distance  $d$  from Star A. Photons from Star B encounter the jet at an angle  $\cos\theta_* = r/\sqrt{r^2 + d^2}$ .

where we have used fiducial LFs  $\Gamma = 300\Gamma_{2.5}$ ,  $\gamma_e = 10^2\gamma_{e,2}$ , and

$$\eta_{KN} = \min\left(1, \frac{1.7}{\Gamma_{2.5}\gamma_{e,2}\epsilon_{0,1}}\right) \quad (19)$$

describes the degree to which EIC scattering is KN suppressed. Suppose the jet is launched steadily with (isotropic) power  $L_j = 10^{53} \text{ erg/s } L_{j,53}$  and duration  $T_j = 10s T_{j,1}$ , so the total (isotropic) kinetic energy is  $E_j = 10^{54} \text{ erg } E_{j,54}$  and the thickness of the jet is  $\Delta r = cT_j = 3 \times 10^{11} \text{ cm } T_{j,1}$ . Considering possible KN suppression, we estimate the EIC optical depth of the whole jet as

$$\tau_j(r) \simeq \frac{E_j \sigma_T}{4\pi r^2 \Gamma m_p c^2} \eta_{KN} \quad (20)$$

The jet becomes transparent to external photons at radius

$$r_{tr} \simeq 3.4 \times 10^{14} \text{ cm } \sqrt{\frac{E_{j,54}}{\Gamma_{2.5}} \eta_{KN}} \quad (21)$$

Here, to estimate the total number of EIC scattered photons, we consider external photons that are in the  $\pi\theta_{j,max}^2$  solid angle to be swept by the jet ( $\theta_{j,max}$  being the half opening angle of the jet). As the jet sweeps through the volume  $\pi\theta_{j,max}^2 r^2 dr$ , the probability of an external photon being scattered by the jet is  $\min(1, r_{tr}^2/r^2)$ . This is because: below  $r_{tr}$ , the jet is optically thick and all the external photons contribute to the EIC flux; above  $r_{tr}$ , the effective cross section of the jet is the sum of individual electrons and that equals to  $\pi\theta_{j,max}^2 r_{tr}^2$  and is smaller than  $\pi\theta_{j,max}^2 r^2$ . Note that  $r_{tr}$  in Eq.(21) is different from the photospheric radius in that the former considers all electrons in the jet but the latter only considers electrons in the casualty connected thickness  $r/2\Gamma^2$  (usually  $\ll cT_j$ ). We note the fact that EIC flux from outside the casualty connected region (deeper layers in the jet) will arrive at the observer at later time, and this is fully taken into account when we calculate the spectra and lightcurves (through Eq. 16).

The number density of external soft photons is given by

$$n_\gamma = \frac{L_b}{4\pi(r^2 + d^2)\epsilon_0 c} \quad (22)$$

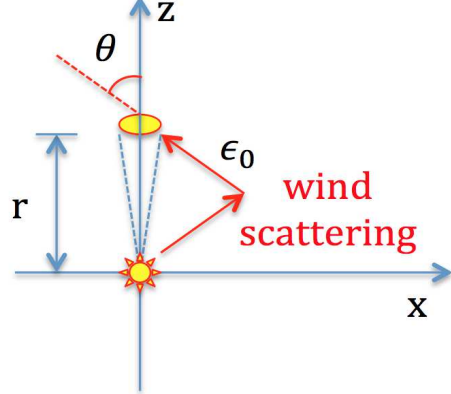


**Figure 4.** Geometry of Case (II). The jet is on the z axis at a distance  $r$  from the progenitor star. Photons originally from Star A are scattered first by electrons in the wind and again by the jet. The wind scattered photons encounter the jet with an angle  $\theta$ .

The total (isotropic) number of scattered photons is

$$N_\gamma = \int_0^\infty (1 - \beta \cos\theta_*) n_\gamma(r, d) \min(1, \tau_j(r)) 4\pi r^2 dr \quad (23)$$

from which, we can easily see that most photons are scattered at radius  $r \sim d$ . Therefore, we can estimate

$$N_\gamma \sim 3 \times 10^{53} \frac{L_{b,39} d_{15}}{\epsilon_{0,1}} \min\left(1, \frac{r_{tr}^2}{d^2}\right) \quad (24)$$

Multiplying  $N_\gamma$  by the scattered photons' energy from Eq.(18), we get the total EIC energy

$$E_{EIC} \sim 4 \times 10^{51} \text{ erg } \Gamma_{2.5}^2 \gamma_{e,2}^2 \eta_{KN} L_{b,39} d_{15} \min\left(1, \frac{r_{tr}^2}{d^2}\right) \quad (25)$$

Note that the estimate is not accurate when  $r_{tr} \gg d$ , because the soft photons are moving nearly parallel to jet, and hence both  $N_\gamma$  and  $\epsilon$  decrease by orders of magnitude.

### 3.1.2 Case (II) — Stellar Wind

As suggested by e.g. Woosley (1993) and MacFadyen & Woosley (1999), GRB progenitor stars are possibly Wolf-Rayet (W-R) stars, which have a typical mass loss rate of  $10^{-5} M_\odot/\text{yr}$ , bolometric luminosity  $10^{39} \text{ erg/s}$ , and effective temperature  $10^5 \text{ K}$  (Crowther 2007). We consider that photons originally from the progenitor star are scattered first by the wind and then by the jet. The geometry is shown in Fig.(4).

We assume a steady wind and denote the wind velocity<sup>5</sup> as  $v = 10^8 \text{ cm/s } v_8$  and the mass loss rate as  $\dot{M} = 10^{-5} M_\odot/\text{yr } \dot{M}_{-5}$ . The wind-scattering optical depth of the region with radius  $> r$  is

$$\begin{aligned} \tau_{wind}(r) &= \sigma_T \int_r^\infty \frac{\dot{M}}{4\pi \tilde{r}^2 v m_p c^2} d\tilde{r} \\ &\simeq 2 \times 10^{-3} \frac{\dot{M}_{-5}}{v_8} r_{14}^{-1} \end{aligned} \quad (26)$$

<sup>5</sup> The order of escape velocity.

Therefore, the wind-scattered photon density is

$$n_\gamma(r) = \frac{L_b \tau_{wind}(r)}{4\pi r^2 \epsilon_0 c} (\propto r^{-3}) \quad (27)$$

The number of scattered photons has a logarithmic dependence on  $r$  when  $r < r_{tr}$ , and then drops off as  $r^{-2}$  at larger radius, so we can estimate the total (isotropic) number of scattered photons as

$$N_\gamma = 2.9 \times 10^{51} \frac{L_{b,39} \dot{M}_{-5}}{\epsilon_{0,1} v_8} \ln \left( \frac{r_{tr,14}}{R_{*,11}} \right) \quad (28)$$

where  $R_* = 10^{11} \text{ cm}$   $R_{*,11}$  is the radius of the star. Therefore, the total EIC energy is

$$E_{EIC} = 4.2 \times 10^{49} \text{ erg} \frac{L_{b,39} \dot{M}_{-5} \Gamma_{2.5}^2 \gamma_{e,2}^2 \eta_{KN}}{v_8} \ln \left( \frac{r_{tr,14}}{R_{*,11}} \right) \quad (29)$$

### 3.1.3 Case (III) — Star Cluster

Consider the GRB progenitor star being in a young massive cluster. All the stars in the cluster create a nearly isotropic and uniform EPF around the GRB jet. Scattering by electrons accelerated by both internal dissipation (ID) and external shocks (ES) may be important. We assume that the cluster has a(n) (O-)star density of  $n_* = 10^4 \text{ pc}^{-3}$   $n_{*,4}$  and a radius of  $R = 1 \text{ pc}$   $R_{pc}$ . We assume stars have an average bolometric luminosity of  $L_b = 10^{39} \text{ erg/s}$   $L_{b,39}$  and peak energy  $\epsilon_0 = 10 \text{ eV}$   $\epsilon_{0,1}$ . The number density of EPF can be estimated as

$$n_\gamma \simeq \frac{n_* L_b R}{\epsilon_0 c} \simeq 2 \times 10^6 \text{ cm}^{-3} \frac{n_{*,4} L_{b,39} R_{pc}}{\epsilon_{0,1}} \quad (30)$$

First, we consider ID. After the jet becoming transparent ( $r > r_{tr}$ ),  $4\pi r^2 n_\gamma \tau_j$  is a constant. The total number of scattered photons depends on the largest radius where electrons stay hot  $r_{max}$ , which is quite uncertain (Piran 2004; Mészáros 2006; Kumar & Zhang 2015). Observationally, the duration of GRB prompt emission ( $T_{90}/(1+z) \sim 10 \text{ s}$ ) gives an upper limit of the radius where the ID is active

$$r_{ID} \leq 2\Gamma^2 c T_{90}/(1+z) \simeq 5 \times 10^{16} \text{ cm} \Gamma_{2.5}^2 \quad (31)$$

Theoretically, an upper limit of  $r_{ID}$  is the deceleration radius  $r_{dec}$  (see Eq.37 below), where the jet starts to decelerate substantially. Note that, after the prompt emission is produced, electrons cool via adiabatic expansion  $\gamma_e \propto r^{-2/3}$  and may stay hot for some time. Putting the uncertainties in the parameter  $r_{max} = 10^{16} \text{ cm}$   $r_{max,16}$ , we estimate the total EIC energy by

$$\begin{aligned} E_{EIC} &\simeq (\epsilon \tau_j n_\gamma 4\pi r^3/3)|_{r=r_{max}} \\ &\simeq 1.4 \times 10^{50} \text{ erg} E_{j,54} \Gamma_{2.5}^2 \gamma_{e,2}^2 \eta_{KN}^2 \\ &\quad \cdot n_{*,4} L_{b,39} R_{pc} \cdot r_{max,16} \end{aligned} \quad (32)$$

Next, we consider the EIC emission from ES, where both the reverse shocked (RS) and forward shocked (FS) region may contribute significantly. EIC emission from ES strongly depends on the ES dynamical evolution.

We assume pressure equilibrium<sup>6</sup> between FS and RS

<sup>6</sup> This may only hold for a so-called short-lived RS, but see Uhm (2011) for a description of a long-lived RS, where RS may reach a much larger radius. Then the EIC energy from RS could be much larger.

region (Kobayashi 2000), both moving together with LF  $\Gamma_{sh}$ . Then  $\Gamma_{sh}$  is only a function of jet LF  $\Gamma$  and the density ratio  $n/n_{ej}$ , where  $n$  is the number density of the circum-burst medium and  $n_{ej}$  is the comoving number density of unshocked ejecta. Before RS crosses the jet, the LF of the shocked region is

$$\Gamma_{sh}(r) = \frac{\Gamma}{(1 + 2\Gamma \sqrt{n(r)/n_{ej}(r)})^{1/2}} \quad (33)$$

The comoving number density of the unshocked ejecta is

$$n'_{ej}(r) = \frac{E_j}{4\pi r^2 T_j \Gamma^2 m_p c^3} \quad (34)$$

The circum-burst medium is either a uniform density medium or stratified like a wind ( $n \propto r^{-2}$ ) out to the wind termination shock radius. GRB afterglow analyses suggest that about half of the long GRBs have a uniform or weak (1/100 W-R) wind density profile, rather than a normal W-R wind profile (e.g. Panaitescu & Kumar 2001; Chevalier et al. 2004), the reason for which is still an open question.

For simplicity, we take the electrons' number density in the cluster to be uniform  $n = 10 \text{ cm}^{-3}$   $n_1$ . Then the jet dynamics is characterized by the deceleration radius  $r_{dec}$  (see e.g. Piran 2004). At radius  $r < r_{dec}$ , whether RS is relativistic ( $\Gamma_{sh} \ll \Gamma$ ) or Newtonian ( $\Gamma_{sh} \approx \Gamma$ ) depends on the factor in Eq.(33)  $2\Gamma(n/n_{ej})^{1/2} \simeq 0.48 \Gamma_{2.5}^2 r_{17} (n_1 T_{j,1}/E_{j,54})^{1/2}$ . For a fast jet, say  $\Gamma \geq 10^3$ , from Eq.(33), we have

$$\Gamma_{sh}(r) \simeq 1.4 \times 10^2 r_{17}^{-1/2} \left( \frac{E_{j,54}}{n_1 T_{j,1}} \right)^{1/4} (\ll \Gamma) \quad (35)$$

For a slow jet, say  $\Gamma = 100$ ,  $2\Gamma(n/n_{ej})^{1/2} \ll 1$ , so we have  $\Gamma_{sh}(r \leq r_{dec}) \simeq 100$ .

The deceleration radius can be estimated by

$$\Gamma_{sh}^2 \frac{4\pi}{3} r_{dec}^3 n m_p c^2 = E_j/2 \quad (36)$$

which gives

$$r_{dec} \simeq 9.3 \times 10^{16} \text{ cm} \frac{E_{j,54}^{1/3}}{\Gamma_{sh,2}^{2/3} n_1^{1/3}} \quad (37)$$

Therefore, for a jet LF  $\Gamma \in (10^2, 10^3)$ , we always have  $r_{dec} \sim 10^{17} \text{ cm}$  and  $\Gamma_{dec} \equiv \Gamma_{sh}(r_{dec}) \sim 100$ . Hereafter we use  $r_{dec} = 10^{17} \text{ cm}$   $r_{dec,17}$  and  $\Gamma_{dec} = 10^2 \Gamma_{dec,2}$  as the fiducial values.

Electrons in the RS and FS region are accelerated to different LFs. Assuming a fraction  $\epsilon_e$  of the shocked fluid's internal energy goes into electrons, we have

$$\gamma_e \simeq \begin{cases} \epsilon_{e,r} \frac{1}{2} \left( \frac{\Gamma}{\Gamma_{sh}} + \frac{\Gamma_{sh}}{\Gamma} \right) \frac{m_p}{m_e} & \text{(RS)} \\ \epsilon_{e,f} \Gamma_{sh} \frac{m_p}{m_e} & \text{(FS)} \end{cases} \quad (38)$$

where  $m_p$  and  $m_e$  are proton and electron mass. Below, we consider RS and FS separately.

(1) *RS*: EIC emission from RS peaks when RS crosses the end of the jet. After shock crossing, a rarefaction wave propagates through the RS region at sound speed and decreases the internal energy substantially. Despite the difference between shock crossing time (slightly earlier, typically) and deceleration time (later), a good approximation is that RS region stays hot until  $r_{dec}$ . The energy equipartition parameter  $\epsilon_{e,r}$  is poorly constrained from GRB afterglows,

**Table 1.** Summary of the EIC emission from our analytical calculation (Section 3.1, not considering pair-production absorption and electrons having a single LF), including  $h\nu_p$  (**peak energy**),  $L_{EIC}^{iso}$  (**isotropic EIC luminosity**),  $t_{obs}$  (**duration of EIC luminosity**),  $N_{EIC}^{iso}$  (**isotropic number of EIC photons at  $\sim \nu_p$** ). The scaled parameters are all set to 1, including  $E_{j,54}$  (isotropic jet kinetic energy),  $T_{j,1}$  (jet duration),  $\Gamma_{2.5}$  (jet bulk LF),  $\gamma_{e,ID,2}$  (ID-accelerated electrons' LF),  $r_{max,16}$  (the maximum radius electrons stay hot),  $\Gamma_{dec,2}$  (bulk LFs of FS and RS at deceleration radius),  $\gamma_{e,RS,2.5}$  (RS-accelerated electrons' LF),  $r_{dec,17}$  (deceleration radius),  $T_{4.7}$  (temperature of EPF-contributing stars),  $L_{b,39}$  (bolometric luminosity of EPF-contributing stars),  $M_{-5}$  (wind mass loss rate),  $v_8$  (wind velocity),  $n_{*,4}$  (stellar number density in the cluster),  $R_{pc}$  (radius of the cluster).

Cases	I ( $d = 10^{14}$ )	I ( $d = 10^{15}$ )	I ( $d = 10^{16}$ )	II	III (ID)	III (RS)	III (FS)
$h\nu_p$ [GeV]	9	9	9	9	9	9	26
$L_{EIC}^{iso}$ [erg/s]	$4 \times 10^{49}$	$5 \times 10^{49}$	$5 \times 10^{48}$	$5 \times 10^{48}$	$10^{49}$	$5 \times 10^{48}$	$2 \times 10^{46}$
$t_{obs}$ [s]	10	10	10	10	10	$2 \times 10^2$	$2 \times 10^4$
$N_{EIC}^{iso}$ <sup>a</sup>	$3 \times 10^{52}$	$3 \times 10^{52}$	$3 \times 10^{51}$	$3 \times 10^{51}$	$10^{52}$	$10^{53}$	$6 \times 10^{51}$
$r_{eff}$ <sup>b</sup> [cm]	$d(10^{14})$	$d(10^{15})$	$d(10^{16})$	$r_{tr}(3 \times 10^{14})$	$r_{max}(10^{16})$	$r_{dec}(10^{17})$	$r_{KN}(3.3 \times 10^{17})$

<sup>a</sup>  $10^{52}$  photons from 1 Gpc ( $z = 0.25$ ) give a photon fluence of  $10^{-4} \text{ cm}^{-2}$ . With a collecting area  $\sim 10^4 \text{ cm}^2$ , *Fermi* Large Area Telescope (LAT) is capable of probing the EPF around low-redshift ( $z \lesssim 0.5$ ) GRB progenitor stars. Also note that the EIC photons from the forward shock in *Case (III)* span a large range of energies. The isotropic number of EIC photons in 0.1 – 300 GeV (*Fermi* LAT sensitivity range) is  $N_{EIC}^{iso} \simeq 2.5 \times 10^{53}$  and the duration is  $t_{obs} \simeq 9 d$  (see Section 3.1.3).

<sup>b</sup> By using a constant  $\gamma_e$  at all radius in our analytical and numerical calculations, we are making an assumption that electrons are hot near the radius  $r_{eff}$  where most scatterings happen (see Fig.6 for a justification).

since there are not many confirmed RS detections. Considering the uncertainties, we use  $\epsilon_{e,r} = 0.1$  (the same as in FS). Therefore, from Eq.(38), we get  $\gamma_e \simeq 1.8 \times 10^2 (1 + \Gamma/2\Gamma_{sh})$ , i.e. typically a few hundred. Hereafter, we use  $\gamma_e = 300\gamma_{e,2.5}$  as the fiducial value for RS.

According to Eq.(18), the scattered photons' energy is  $\epsilon \simeq 9\text{GeV} \Gamma_{dec,2}^2 \gamma_{e,2.5}^2 \epsilon_{0,1}$  (marginally KN suppressed) and the total (isotropic) EIC energy from RS can be estimated as

$$E_{EIC}^{RS} = (\epsilon \tau_j n_\gamma 4\pi r^3 / 3)|_{r=r_{dec}} \quad (39)$$

$$\simeq 1.4 \times 10^{51} \text{ erg} \frac{E_{j,54}}{\Gamma_{2.5}} n_{*,4} L_{b,39} R_{pc} \Gamma_{dec,2}^2 \gamma_{e,2.5}^2 r_{dec,17}$$

(2) *FS*: We use Eq.(38) with a constant  $\epsilon_e = 0.1$  (Panaitescu & Kumar 2001) to get the electrons' LF  $\gamma_e$ . At  $r_{dec}$ , EIC radiation from FS region is strongly KN suppressed, so the total EIC energy is rising with  $r$  ( $E_{EIC}^{FS} \propto r^4$  as shown below), until the scattering changes from KN to Thomson regime. The characteristic radius where this transition happens is denoted as  $r_{KN}$ , given by

$$\Gamma_{sh}(r_{KN}) \gamma_e \epsilon_0 = m_e c^2 \quad (40)$$

After  $r_{dec}$ , we expect the Blandford-McKee evolution (Blandford & McKee 1976)

$$\Gamma_{sh}(r) \simeq \Gamma_{dec} \left( \frac{r}{r_{dec}} \right)^{-3/2} \quad (41)$$

Putting Eq.(38) and (41) to Eq.(40), we get the ‘‘KN radius’’

$$r_{KN} \simeq 3.3 r_{dec} \Gamma_{dec,2}^{2/3} \epsilon_{0,1}^{1/3} \quad (42)$$

We know  $E_{EIC}^{FS} \propto \epsilon \tau_{FS} r^3$ . When  $r_{dec} < r < r_{KN}$ , the scattered photons' energy  $\epsilon \propto r^{-3}$ , and the optical depth of FS region  $\tau_{FS} \propto r^4$ , so we get  $E_{EIC}^{FS} \propto r^4$ . In a similar way, when  $r > r_{KN}$ , we get  $E_{EIC}^{FS} \propto r^{-2}$ . Therefore, most EIC

energy is produced at radius  $r_{KN}$ , and we obtain

$$E_{EIC}^{FS} \simeq (\epsilon \tau_{FS} n_\gamma 4\pi r^3 / 3)|_{r=r_{KN}} \quad (43)$$

$$\simeq 2.6 \times 10^{50} \text{ erg} \frac{n_{*,4} L_{b,39} R_{pc}}{\epsilon_{0,1}^{2/3}} n_1 r_{dec,17}^4 \Gamma_{dec,2}^{8/3}$$

where we have used  $\epsilon(r_{KN}) \simeq (m_e c^2)^2 / \epsilon_0 = 26\text{GeV} \epsilon_{0,1}^{-1}$  and  $\tau_{FS}(r_{KN}) \simeq r_{KN} n \sigma_T / 3$ . We note the strong dependence on both  $r_{dec}$  and  $\Gamma_{dec}$ . Also, higher energy (up to  $\sim \text{TeV}$ ) EIC photons are produced at radius  $r_{dec} < r < r_{KN}$ , but they contribute a smaller EIC energy. At radius  $r > r_{KN}$ , the decreasing of EIC energy  $E_{EIC}^{FS} \propto r^{-2}$  is mostly due to the fast decreasing of EIC photons' energy  $\epsilon \propto \Gamma^4 \propto r^{-6}$ . On the other hand, the total isotropic number of EIC photons is rising with radius  $N_{EIC}^{iso} = 4\pi r^3 \tau_{FS} n_\gamma / 3 \propto r^4$  and so as the observational duration  $t_{obs} \propto r / \Gamma^2 \propto r^4$ . Therefore, if we use the the same fiducial parameters as in Eq.(43), (1) the total isotropic number of photons in the 0.1 – 300 GeV energy range (*Fermi* Large Area Telescope sensitivity) is  $N_{EIC}^{iso}(r_{KN})(26/0.1)^{4/6} \simeq 2.5 \times 10^{53}$ ; (2) the observational duration is  $t_{obs} \simeq (26/0.1)^{4/6} r_{KN} / [2\Gamma_{sh}^2(r_{KN})c] \simeq 9 d$  and the photon number flux is constant with time. Mimica & Giannios (2011) also calculated the EIC scattering of diffuse EPF in a dense star cluster by the forward shock. They used a lower stellar number density and a more realistic circum-burst medium density profile (by simulating the wind-wind collision between a Wolf-Rayet star and an O star), and the results in this paper are consistent with theirs.

### 3.2 Lightcurves and Spectra

In this subsection, we put realistic EPF profiles into the procedure developed in Section 2 and calculate the EIC lightcurves and spectra for the three cases. As a

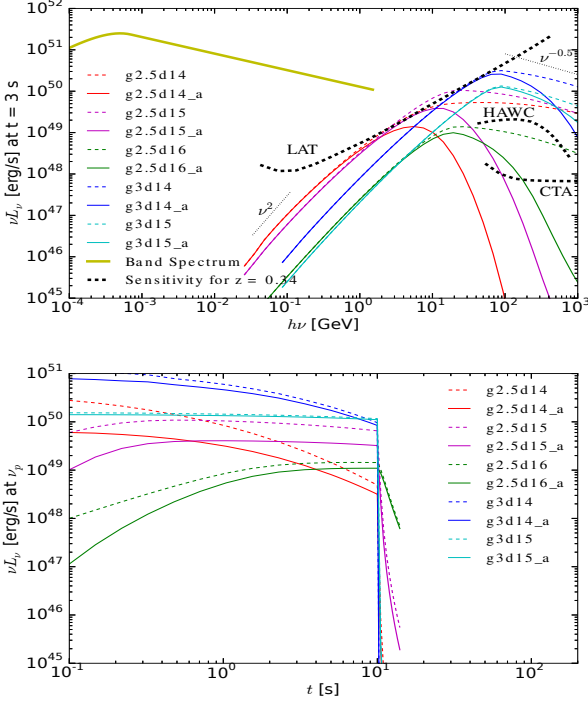


**Figure 5.** Spectra at  $t_{\text{obs}} = 3$  s (upper panel) and lightcurves at  $\nu_p$  in the *Binary Case*, for different binary separations  $d$  and bulk Lorentz factors  $\Gamma$  (e.g. “d14” means  $d = 10^{14}$  cm and “g2.5” means  $\Gamma = 10^{2.5} = 300$ ). ( $\nu_p$ ’s are the peaks of  $\nu L_\nu$  spectra with absorption, solid lines, in the upper panel.) We show the differences between calculations with/without pair-production absorption by using dashed/solid lines (“a” means absorption is included). Absorption is weaker for a larger bulk Lorentz factor or a larger binary separation. The scaled parameters  $E_{j,54}$ ,  $T_{j,1}$ ,  $\gamma_{m,2}$ ,  $T_{4.7}$ ,  $L_{b,39}$  are all set to 1 and the electron power-law index  $p = 2.2$ . The thick yellow line is the “classical” Band spectrum (Band et al. 1993) with  $E_{\text{peak}} = 500$  keV,  $\alpha = -1$ ,  $\beta = -2.4$ ,  $L_{\text{tot}} = 10^{52}$  erg/s. The thick dashed black lines are differential sensitivity of different telescopes. The EIC spectra show  $\nu L_\nu \propto \nu^2$  below  $\nu_p$  and  $\propto \nu^{-0.5}$  above  $\nu_p$ , plus additional high energy softening caused by pair production.

general assumption, in each case, the star(s) that contribute to EPF are assumed to have bolometric luminosity  $L_b = 10^{39}$  erg/s  $L_{b,39}$  and effective temperature  $T = 5 \times 10^4$  K  $T_{4.7}$ , so the specific luminosity is

$$L_{\nu_0} = \frac{\pi L_b}{\sigma_{SB} T^4} \cdot \frac{2h\nu_0^3}{c^2} \frac{1}{e^{h\nu_0/kT} - 1} \quad (44)$$

where  $\sigma_{SB}$  is the Stefan-Boltzmann constant.

(I) *Binary Case*: We consider the companion star as a point source, so the EPF intensity at position  $\vec{r} = (r, \theta_j, \phi_j)$ , in the direction  $(\theta, \phi)$ , is

$$I_{\nu_0}(\vec{r}, \theta, \phi) = \frac{L_{\nu_0}}{4\pi(r^2 + d^2)} \sin\theta_* \delta(\theta - \theta_*) \delta(\phi - \pi) \quad (45)$$

where  $\sin\theta_* = d/\sqrt{r^2 + d^2}$ ,  $d$  is the binary separation, and  $\delta(x)$  is the Dirac- $\delta$  function.

(II) *Wind Case*: Assuming a steady wind with mass loss rate  $\dot{M}$  and speed  $v$ , we get the number density of circumstellar electrons at a distance  $r$  from the center

$$n_e(r) = \frac{\dot{M}}{4\pi r^2 v} \quad (46)$$

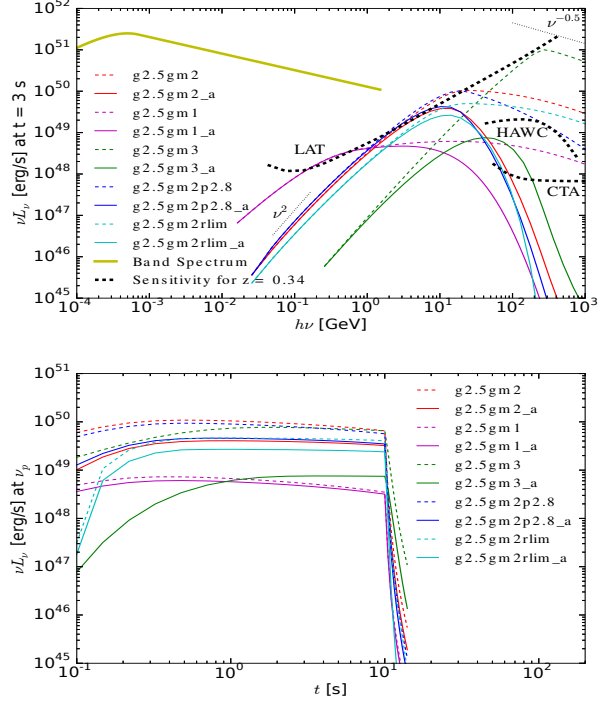


**Figure 6.** Spectra and lightcurves for different jet parameters in the *Binary Case*. In the fiducial case (red),  $E_{j,54}$ ,  $T_{j,1}$ ,  $\Gamma_{2.5}$ ,  $\gamma_{m,2}$ ,  $d_{15}$ ,  $T_{4.7}$ ,  $L_{b,39}$  are all set to 1 and the electron power-law index  $p = 2.2$ . Magenta lines are for  $\gamma_m = 10$ , so the scattered photons have lower energies and the un-absorbed spectrum is slightly rising from 0.3 to  $\sim 10$  GeV, because the scattering is in the Thomson regime ( $\nu L_\nu \propto \nu^{(3-p)/2}$ ). Green lines are for  $\gamma_m = 10^3$ , so the scattered photons reach  $\sim 300$  GeV, but absorption is strong. Blue lines correspond to  $p = 2.8$ , and the only difference from the red lines is that the high energy spectral slope is steeper, approaching  $\nu^{1-p}$  faster because the  $\ln(a\theta)$  term (Eq. 12) plays less of a role. For cyan lines, we assume electrons are hot only in a limited radius range  $r \in (d/2, 2d)$ . The small difference between the red and cyan lines means that, by using a constant  $\gamma_m$  at all radius, we are making an assumption that electrons are hot near the radius where most scatterings happen (see  $r_{eff}$  in Table 1). The yellow line in the upper panel is the “classical” Band spectrum (see Fig.5 for details) shown for comparison.

Then the emissivity from wind scattering is

$$j_{\nu_0}(r) = \frac{n_e(r)\sigma_T}{4\pi r^2} \cdot L_{\nu_0} \quad (47)$$

which is assumed to be isotropic (no dependence on  $\theta$  or  $\phi$ ) from Thomson scattering. The system is spherical symmetric, so  $j_{\nu_0}$  doesn’t depend on  $\theta_j$  or  $\phi_j$ , and hence neither does the intensity  $I_{\nu_0}$ . We integrate along the  $(\theta, \phi)$  direction and get the EPF intensity at position  $\vec{r}$

$$\begin{aligned} I_{\nu_0}(r, \theta, \phi) &= \int_0^\infty j_\nu(r(s)) ds \\ &= 8.0 \times 10^9 \frac{\dot{M}_5}{v_8} \frac{\pi - \theta + \sin\theta \cos\theta}{\sin^3\theta} \frac{L_{\nu_0}}{r^3} \end{aligned} \quad (48)$$

which is independent of  $\phi$ , due to symmetry. Note that the function  $f(\theta) = (\pi - \theta + \sin\theta \cos\theta)/\sin^3\theta \simeq 2(\pi - \theta)^2/3 \rightarrow$



0 when  $\theta \rightarrow \pi^-$  and  $f(\theta) \simeq \theta^{-3} \rightarrow \infty$  (diverges<sup>7</sup>) when  $\theta \rightarrow 0^+$ . However, photons with  $\theta < 1/\Gamma$  are moving nearly parallel to the jet and hence don't contribute significantly to the spectra.

(III) *Star Cluster Case*: All the stars in the cluster create a more or less uniform and isotropic EPF, so the intensity can be estimated as

$$I_{\nu_0} \simeq \frac{n_* L_{\nu_0} R_c}{4\pi} \quad (49)$$

where  $n_*$  is the number density of stars and  $R_c$  is the radius of the cluster.

In Fig.(5)-(8), we present the lightcurves and spectra for the three cases, assuming electrons are accelerated by internal dissipation. Then we discuss the prospects of detecting the predicted high energy photons. We show the representative spectra (upper panels) at observer's time  $t_{obs} = 3$  s for *Case (I)*,  $t_{obs} = 1$  s for *Case (II)*, and  $t_{obs} = 10$  s for *Case (III)*. Since the overall flux levels of the spectra change with time (but the shapes change very little), the different  $t_{obs}$ 's we have chosen are when the spectra have their average amplitudes. By integrating the representative spectra over the duration of EIC emission  $\sim T_j = 10$  s, we obtain the total fluence approximately. The jet parameters  $E_{j,54} = 1$ ,  $T_{j,1} = 1$ ,  $\Gamma_{2.5} = 1$ ,  $\gamma_{m,2} = 1$  and  $p = 2.2$  are our fiducial values in all three cases. To explore the effect of varying jet parameters on EIC emission, we also show the results for a number of different parameters (one at a time):  $\Gamma = 1000$  ( $\Gamma_3 = 1$ ),  $\gamma_m = 10$  ( $\gamma_{m,1} = 1$ ),  $\gamma_m = 1000$  ( $\gamma_{m,3} = 1$ ) and  $p = 2.8$ . For each set of parameters, the solid (dashed) line is when pair-production absorption with GRB prompt emission is (not) considered. Then we measure the peak frequency  $\nu_p$  of the solid line (with absorption) for each set of parameters. The lightcurves (shown in lower panels) are calculated at  $\nu_p$ . In this way, the solid-line lightcurves are close to bolometric and we can see how strong the absorption is at  $\nu_p$ .

To demonstrate the detectability of the IC emission, (1) along with the EIC spectra, we also plot the ‘‘classical’’ prompt emission, i.e. Band spectrum (Band et al. 1993), with  $E_{peak} = 500$  keV,  $\alpha = -1$ ,  $\beta = -2.4$ ,  $L_{tot} = 10^{52}$  erg/s. It's still an open question whether the Band spectrum extends to a few GeV without a cutoff. In some cases, the EIC emission is only observable if Band spectrum has a GeV cutoff. (2) We show in Fig.(5)-(8) the sensitivity of *Fermi* Large Area Telescope (LAT, Atwood et al. 2009), High Altitude Water Cherenkov (HAWC, Abeysekara et al. 2012) observatory, Cherenkov Telescope Array (CTA, Inoue et al. 2013) with integration time 10 s for a GRB at redshift  $z = 0.34$ , which is the redshift of the nearest LAT detected GRB (130427a, Ackermann et al. 2014).

The sensitivity of *Fermi* LAT is calculated using  $\nu F_{\nu}|_{min} = h\nu N_{ph}/(A_{eff}(\nu) * t_{intg})$ , where  $N_{ph} = 1$  is the minimum number of photons,  $t_{intg} = 10$  s is the integration time, and  $A_{eff}(\nu)$  is the detector's effective area (for

<sup>7</sup> The divergence is caused by the assumption of the star being a point source. If we denote the progenitor star's radius as  $R_*$ , at an angle  $\theta < \arcsin(R_*/r)$ , photons come directly from the star. However, as long as the star is not a giant ( $R_* < 10^{13}$  cm), the photons directly from the star are moving nearly parallel to the jet and are hence negligible.

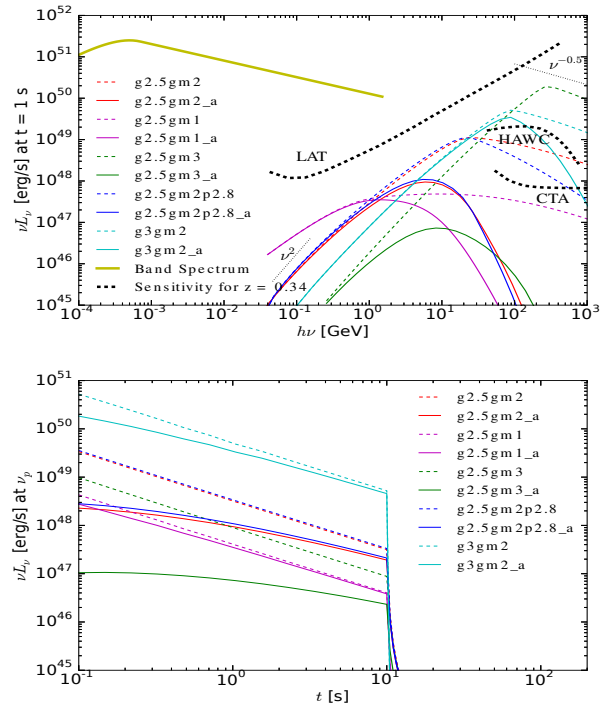


**Figure 7.** Spectra and lightcurves for different jet parameters in the *Wind Case*. In the fiducial case (red),  $E_{j,54}$ ,  $T_{j,1}$ ,  $\Gamma_{2.5}$ ,  $\gamma_{m,2}$ ,  $T_{4.7}$ ,  $L_{b,39}$ ,  $\dot{M}_{-5}$ ,  $v_8$  are all set to 1 and the electron powerlaw index  $p = 2.2$ . Magenta lines correspond to  $\gamma_m = 10$ , and the scattered photons have lower energies. Green lines are for  $\gamma_m = 10^3$ , so the scattered photons reach  $\sim 300$  GeV but the absorption is strong. Blue lines correspond to  $p = 2.8$ , and the only difference from the red lines is that the high energy spectral slope is steeper, approaching  $\nu^{-1-p}$  faster because the  $\ln(a\theta)$  term (Eq. 12) plays less of a role. Cyan lines are for  $\Gamma = 1000$ . The yellow line in the upper panel is the ‘‘classical’’ Band spectrum (see Fig.5 for details) shown for comparison.

‘‘source’’ class photons at normal incidence, Atwood et al. 2009). Considering background and non-normal incidence angles, the true sensitivity of *Fermi* LAT is worse than shown here. We can see that *Fermi* LAT doesn't have enough collecting area to effectively constrain the EIC emission parameters for GRB with  $z \gtrsim 0.34$ . However, HAWC and CTA will be sensitive enough.

Abeysekara et al. (2015) calculate the HAWC (-300) sensitivity with integration time  $t_{intg} = 21.5$  s, and we scale their results for the main data acquisition system by  $t_{intg}^{0.7}$  and obtain the sensitivity for 10 s integration time. As for the CTA sensitivity, we follow the procedure of Bernlöhner et al. (2013) and calculate the minimum flux level of CTA South that satisfies the following three conditions: significance level  $\sigma \geq 5$ , there are at least 10 signal events, and the signal is at least 5% of the remaining background in the direction of the source.

A summary of our numerical results is as follows:

(1) EIC emission is concentrated in 1 - 100 GeV band. The EIC energy is typically  $10^{48} \sim 10^{51}$  erg (hence lu-

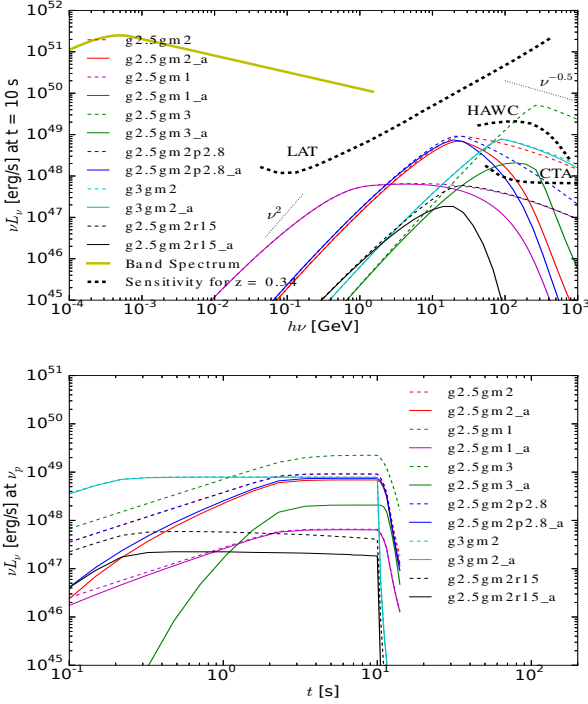


**Figure 8.** Spectra and lightcurves for different jet parameters in the *Star Cluster Case*. In the fiducial case (red),  $E_{j,54}$ ,  $T_{j,1}$ ,  $\Gamma_{2.5}$ ,  $\gamma_{m,2}$ ,  $T_{4.7}$ ,  $L_{b,39}$ ,  $r_{max,16}$ ,  $n_{*,4}$ ,  $R_{pc}$  are all set to 1 and the electron powerlaw index  $p = 2.2$ . Magenta lines correspond to  $\gamma_m = 10$ , so the scattered photons have lower energies and the un-absorbed spectrum is slightly rising from 0.3 to  $\sim 10$  GeV, because the scattering is in the Thomson regime. Green lines are for  $\gamma_m = 10^3$ , so the scattered photons reach  $\sim 300$  GeV, but the absorption is strong. Blue lines correspond to  $p = 2.8$ , and the only difference from the red lines is that the high energy spectral slope is steeper, approaching  $\nu^{1-p}$  faster because the  $\ln(a_\theta)$  term (Eq. 12) plays less of a role. Cyan lines are for  $\Gamma = 1000$ . For black lines, the maximum radius that electrons stay hot is  $r_{max} = 10^{15}$  cm. The yellow line in the upper panel is the “classical” Band spectrum (see Fig.5 for details) shown for comparison.

luminosity  $10^{47} - 10^{50}$  erg/s) and the photon fluence is  $10^{-7} \sim 10^{-4}$  cm $^{-2}$  for a typical redshift $^8$   $z = 1$ .

(2) The numerical spectra follow the scaling of the averaged differential cross section (Eq.10) quite well. Without considering pair production, we get  $\nu L_\nu \propto \nu^2$  below  $\nu_p$  and  $\propto \nu^{-0.5}$  above  $\nu_p$ . In the cases where  $\gamma_m = 10$ , a short segment of  $\nu L_\nu \propto \nu^{(3-p)/2}$  can be seen, because the scattering is in the Thomson regime. At higher energy, the spectra become increasingly steeper and the expected  $\nu^{1-p}$  slope only shows at  $\sim$  TeV. However, pair production usually makes the high energy tail much softer.

(3) The observational challenge is that the EIC emission from the internal dissipation arrives within  $\sim 10$  s of the GRB trigger, which requires that the GRB occurs in the large field of view of a telescope, e.g. *Fermi* LAT,

HAWC and wide-field-mode CTA. However, in the *Star Cluster Case*, although not shown in the figures, EIC photons from the reverse shock will arrive at deceleration time  $t_{dec} = r_{dec}/(2c\Gamma_{dec}^2) \sim 200$  s and those from the forward shock will arrive at the time when the scattering changes from KN to Thomson regime  $t_{KN} = r_{KN}/[2c\Gamma_{sh}(r_{KN})^2] \sim 2 \times 10^4$  s. This gives enough time for some telescopes, e.g. CTA (Inoue et al. 2013), MAGIC (Albert et al. 2007), H.E.S.S. (Aharonian et al. 2009), VERITAS (Acciari et al. 2011), to carry out follow-up observations.

(4) In the *Binary Case*, the strongest EIC emission is expected when  $d \sim 10^{14} - 10^{16}$  cm. Therefore, observations can probe the existence and properties of a possible luminous companion in this distance interval, as long as electrons are hot at radius  $r \sim d$ . Many GRBs have been detected in the 0.1 – 300 GeV band (Ackermann et al. 2013), but the radiation mechanism of the GeV photons during the early prompt emission phase is still uncertain (Kumar & Zhang 2015), so the observed data points can be used as upper limits unless different components can be separated and subtracted. Among all the low redshift GRBs with LAT GeV data, GRB 130427a ( $z = 0.34$ , Ackermann et al. 2014) provides the most stringent constraints. However, for the most favorable jet parameters, the quantum limit of LAT is still slightly above the predicted fluxes. Therefore, the constraints from LAT are weak. For example, assuming jet parameters and binary separations as in red, magenta and blue lines in Fig. 5, we can rule out a companion star with luminosity  $> 5 \times 10^{39}$  erg s $^{-1}$ . On the other hand, HAWC observatory should have been able to put strong constraints on the external photon field around the progenitor of GRB 130427a. Unfortunately, the burst occurred under unfavorable observational conditions (much smaller effective area, Abeysekara et al. 2015). For example, non-detections under normal observational conditions would rule out a companion star of luminosity  $> 3 \times 10^{38}$  erg s $^{-1}$  at  $d \in (10^{14}, 10^{15}$  cm), if  $\Gamma \gtrsim 500$  and  $\gamma_m \simeq 100$ .

We note that, in a possible binary Population III (Pop III) star system, the luminosity of the companion star could be as high as  $10^{40}$  erg/s (Heger & Woosley 2002). A Pop III GRB could also have a higher jet kinetic energy  $E_{j,54} = 10$  (Suwa & Ioka 2011). If a GRB happens in a Pop III binary system $^9$  where the separation between stars is  $d = 10^{15}$  cm, for our fiducial parameters, we expect  $N_{EIC}^{iso} \simeq 2 \times 10^{53}$  at  $\nu_p/(1+z) \sim 8/(1+z)$  GeV, which means a photon fluence of  $\sim 10^{-7}$  cm $^{-2}$  at redshift  $z = 15$  and that could be observed by future large space telescopes.

(5) In the *Wind Case*, EIC emission is usually weak ( $E_{EIC} \sim 10^{49}$  erg), and observations by LAT are not very constraining. Since  $E_{EIC} \propto L_b \dot{M}$  (Eq.29), this case is worth considering because of two possible enhancement channels. First, there might be a persistent (months to years) and strong ( $10^{-3} \sim 1 M_\odot/yr$ ) pre-burst mass loss, as seen in some Type Ibc and all Type IIn supernovae (SNe, e.g. Foley et al. 2007; Smartt 2009; Kiewe et al. 2012). We also

$^8$  The luminosity distance  $D_{L,z=1} = 2.0 \times 10^{28}$  cm from  $D_L = c(1+z)/H_0 \int_0^z dx/\sqrt{\Omega_m(1+x)^3 + \Omega_\Lambda}$ , and  $\Omega_m = 0.27$ ,  $\Omega_\Lambda = 0.73$ ,  $H_0 = 71$  km s $^{-1}$  Mpc $^{-1}$ .

$^9$  The multiplicity and binary separation distribution of Pop III stars are largely unknown. By simulating the growth and evolution of Pop III stellar systems in a sample ( $N = 10$ ) of minihalos, Stacy & Bromm (2013) find a binary fraction of  $\sim 35\%$  (at birth) and that the binary separation (at birth) peaks at  $10^2$  AU. The subsequent evolution of these binary systems is still unexplored.

note that the strong mass loss might not be isotropic<sup>10</sup> and hence could leave no footprints on the afterglow dynamics. Second, an unusually high stellar luminosity might be produced by, e.g. a SN slightly earlier than the GRB, or a hot cocoon<sup>11</sup> surrounding the jet.

(6) In the *Star Cluster Case*, the EIC emission from internal dissipation is weaker than the *Binary Case* by a factor of  $\sim 10$ . We emphasize the importance of EIC radiation from the external shock (ES), because we have a better understanding of the ES than of the internal dissipation in that the standard (low energy) GRB afterglows are most likely due to synchrotron radiation from the ES-accelerated electrons (e.g. Piran 2004). However, the uncertainties of the EIC emission from ES come from the jet dynamical evolution, which depends on circum-burst number density and jet power. Also, GeV emission from other mechanisms needs to be separated, e.g. synchrotron and synchrotron self-Compton emission from forward shock (see Kumar & Zhang 2015, for a review). We predict photon fluence from  $10^{-6} \text{ cm}^{-2}$  (forward shock,  $\sim 30 \text{ GeV}$ ) to  $10^{-5} \text{ cm}^{-2}$  (reverse shock,  $\sim 10 \text{ GeV}$ ) at redshift  $z = 1$ , using our fiducial parameters. Future large telescopes may be able to constrain the properties of the cluster.

## 4 DISCUSSION

In this section, we discuss some potential issues of the EIC emission proposed in this paper.

(1) We note that high energy  $\gamma$ -rays can't propagate through cosmological distances, due to pair production with extragalactic background light (consisting mostly of cosmic infrared, optical and UV backgrounds). Photons of energy  $\geq 100 \text{ GeV}$  can only be observed from nearby ( $z \lesssim 1$ ) GRBs (Gilmore et al. 2012). Therefore, constraints on the external photon field will be most effective for low redshift ( $z \lesssim 1$ ) GRBs. We also note that GRBs with low bulk Lorentz factor  $\Gamma \lesssim 300$  will mostly produce  $\lesssim 10 \text{ GeV}$  photons, which could be observed at high redshift.

(2) We assume the jet kinetic power to be steady for a duration  $T_j$ . In reality, GRB prompt lightcurves show multiple emission pulses. Some pulses are smooth but others vary on millisecond timescale, so the jet kinetic power could be episodic and the internal dissipation could happen locally. The EIC emission is also modulated by the radial distribution of external photon field. If most EIC scatterings happen at radii  $\sim r$ , an infinitely thin shell will produce a pulse of width  $\sim 0.2s r_{15}/\Gamma_{2.5}^2$ . Due to limited number of EIC photons from a source located at cosmological distances, telescopes are not sensitive to the variability down to milliseconds. Instead, the observed EIC lightcurve should more or less track the major pulses of the prompt emission, with smoothing on timescales of order  $\sim 0.2s r_{15}/\Gamma_{2.5}^2$ .

(3) In the *Binary Case*, the EIC luminosity is only significant when the binary separation is large ( $d \geq 10^{14} \text{ cm}$ ). Orbital separation distribution derived from spectroscopic

and direct imaging studies are inevitably biased by selection effects and measurement limitations. By measuring radial velocities, Sana et al. (2012) derived (after completeness corrections) the distribution of orbital periods  $f(\log P) \propto (\log P)^{-0.55}$  for  $P = 1.4 - 3200 \text{ d}$  by analyze the O star population of six nearby Galactic open clusters. Also by measuring radial velocities, Kobulnicky et al. (2014) estimated  $f(\log P) \propto (\log P)^{-0.22}$  for  $P = 1.4 - 2000 \text{ d}$  in the Cygnus OB2 Association. Despite the discrepancy (and also uncertainties), both of them pointed out that about 10% of the binary systems have periods  $P > 10^3 \text{ d}$ , which corresponds to  $d \simeq 10^{14} \text{ cm}$ . An even greater uncertainty comes from the unknown nature of GRB progenitors, which may not be O stars (Woosley 1993; MacFadyen & Woosley 1999). Detection of the EIC emission proposed in this paper will shed light on the nature of GRB progenitors.

(4) In the *Star Cluster Case*, the EIC luminosity depends on the number density of massive stars at the time when the GRB occurs. There are large uncertainties in the first few Myr of the star clusters' evolution (see e.g. Portegies Zwart et al. 2010), especially in the so-called Gas Expulsion Stage (GES) during which the residual gas in the cluster is blown away by stellar winds or outflows. The loss of mass during GES will cause the cluster to expand and the shallower potential well may allow a fraction of the stars (especially the ones at outer radius) to escape. Therefore, the overall stellar number density drops with time. Long GRBs are concentrated on the very brightest regions of actively star-forming galaxies, where young massive clusters are particularly abundant (Fruchter et al. 2006). However, little is known about the very nearby ( $\sim 1 \text{ pc}$ ) environment around the long GRB progenitors, and it is unclear whether the stars escaped<sup>12</sup> from the clusters. The EIC signal proposed in this paper could potentially give us some hint. For example, an upper limit of  $L_{EIC} < 10^{49} \text{ erg/s}$  will constrain the number density of massive ( $> 20 - 30M_{\odot}$ ) stars to be  $n_* < 10^4 \text{ pc}^{-3}$ .

(5) There are a few potential issues in our numerical procedures developed in Section 2. (a) We assume electrons are accelerated to ultra-relativistic energies and have a simple powerlaw Lorentz factor (LF) distribution. On one hand, if GRB prompt emission is produced via sub-photospheric Comptonization, then  $\gamma_m$  (or electrons' thermal LF) might be of order a few or less. In that case, the EIC emission would be much weaker than the internal dissipation model considered in this work. On the other hand, even if electrons are accelerated to a simple powerlaw, due to synchrotron, synchrotron-self-Compton, or EIC cooling, there's a cooling LF  $\gamma_c$  above which electrons' distribution turns softer. The resulting EIC spectrum at energy higher than  $\Gamma\gamma_c m_e c^2$  will be softer than our prediction, but the total EIC energy will not change much, as long as  $\gamma_c > \gamma_m$ . (b) Electron's LF distribution is actually evolving with time, i.e.  $\gamma_m$ ,  $\gamma_c$  and possibly the powerlaw index  $p$  are all functions of time (or radius). In principle, by convolving the time dependent LF distribution with single particle emission, we can calculate the EIC emission to a higher degree of accuracy. How-

<sup>10</sup> For example, due to the fast rotation of the progenitor, most of the gas could be ejected near the equatorial plane.

<sup>11</sup> See Kumar & Smoot (2014) for the EIC scattering of the hot cocoon radiation by the GRB jet.

<sup>12</sup> Hammer et al. (2006) found GRB 980425 (the nearest GRB at  $z = 0.008$ , e.g. Galama et al. 1998) to be  $\sim 800 \text{ pc}$  away from the nearby massive star-forming region.

ever, since we are not yet sure where the internal dissipation accelerates electrons and how long will electrons stay hot (Kumar & Zhang 2015), such a detailed calculation is left for possible future investigation. Instead, constant  $\gamma_m$  and  $p$  are used at all radius. As shown in Section 3.2 (Fig.6), by using a constant  $\gamma_m$  at all radius, we are making an assumption that electrons are hot near the radius  $r_{eff}$  where most scatterings happen.

(6) Another interesting application is the IC scattering of the Cosmic Microwave Background (CMB) at high redshift by Pop III GRB jets. The earliest Pop III stars form in minihalos of mass  $\sim 10^6 M_\odot$  at redshift  $z \sim 20 - 30$  (Bromm 2013). The CMB photon number density is

$$n_{CMB} \simeq aT^4/(2.7kT) = 3.3 \times 10^6 [(1+z)/20]^3 \text{ cm}^{-3} \quad (50)$$

where we have used the CMB temperature  $T = 2.7(1+z) = 54K (1+z)/20$  (i.e.  $\epsilon_0 = 4.7 \times 10^{-3} \text{ eV}$ ). The forward shock (FS) is highly relativistic at deceleration radius, and electrons are accelerated to LF  $\gamma_e = 1.8 \times 10^5$  (using  $\epsilon_e = 0.1$ , and  $\Gamma_{dec} = 100$ ). Therefore, EIC emission from the FS could be observed at  $0.8 \text{ GeV } \Gamma_{dec,2}^4$ . If we use a jet kinetic energy  $E_j = 10^{55} \text{ erg}$  (isotropic equivalent) and a uniform circumburst medium density of  $n = 100 \text{ cm}^{-3}$ , we get the deceleration radius  $r_{dec} \simeq 10^{17} \text{ cm}$  (Eq.37). The total (isotropic) number of EIC photons from FS is

$$\begin{aligned} N_{EIC}^{FS} &\simeq (\tau_{FS} n_{CMB} 4\pi r^3/3)|_{r=r_{dec}} \\ &\simeq 3.0 \times 10^{52} [(1+z)/20]^3 n_2 r_{dec,17}^4 \end{aligned} \quad (51)$$

Since  $N_{EIC}^{FS}$  strongly depends on  $r_{dec}$ , a more accurate calculation of the dynamical evolution is needed. Using  $N_{EIC}^{FS} = 3 \times 10^{52}$ , we expect a photon fluence of  $\sim 5 \times 10^{-9} \text{ cm}^{-2}$  at  $\sim 1 \text{ GeV}$  from redshift 20.

(7) Lastly, we estimate the possible contribution of the EIC emission to the extragalactic  $\gamma$ -ray background (EGB) around  $100 \text{ GeV}$ , by the FS channel or ID channel when GRBs have large LF (e.g.  $\Gamma \geq 500$ ). We optimistically estimate the average (isotropic) EIC energy around  $100 \text{ GeV}$  from one GRB to be  $E_{EIC} = 10^{51} \text{ erg}$ . The average (observed) GRB rate in the local ( $z < 1$ ) Universe is estimated by Wanderman & Piran (2010) to be  $\bar{\rho} \sim 3 \text{ Gpc}^{-3} \text{ yr}^{-1}$ . We integrate over the local Universe to  $R_{max} = 4 \text{ Gpc}$  and estimate the intensity of EGB contributed by the EIC channel to be  $I_{EGB} \simeq E_{EIC} \bar{\rho} R_{max}/4\pi \simeq 2 \times 10^{-6} \text{ MeV cm}^{-2} \text{ s}^{-1} \text{ sr}^{-1}$ . The EGB at  $100 \text{ GeV}$  observed by *Fermi* LAT is  $\sim 10^{-4} \text{ MeV cm}^{-2} \text{ s}^{-1} \text{ sr}^{-1}$  (Abdo et al. 2010). Therefore, the EIC channel in GRBs could (at most) contribute a small fraction of EGB. The possible contributions from other GRB channels are estimated by Casanova et al. (2007).

## 5 CONCLUSIONS

GRB progenitors may be surrounded by a significant external photon field (EPF), due to the existence of a massive companion star (*Case I*), a strong stellar wind (*Case II*), or a dense star cluster (*Case III*). We calculate the IC scattering of the EPF (i.e. EIC emission) by the hot electrons in the GRB jet, which could be accelerated by internal dissipation or external shocks. As long as electrons are accelerated to ultra-relativistic powerlaw, the results presented in this

work is independent of the details of jet dissipation mechanism and electron acceleration process.

In each *Case*, the EPF-contributing star(s) are assumed to have bolometric luminosity  $10^{39} \text{ erg/s}$  and effective temperature  $5 \times 10^4 \text{ K}$ . The GRB jet is assumed to have total kinetic energy  $10^{54} \text{ erg}$  (isotropic equivalent), duration  $T_j = 10 \text{ s}$  and bulk Lorentz factor  $\Gamma$ . We assume that electrons are accelerated by internal dissipation to a powerlaw distribution with minimum Lorentz factor  $\gamma_m$  and index  $p$ . We present in this work the EIC lightcurves and spectra for each case, for a variety of EPF and jet parameters ( $\Gamma$ ,  $\gamma_m$  and  $p$ ). We take into account the equal-arrival time surface and possible absorption of high energy photons caused by pair production with the prompt  $\gamma$ -rays.

For our fiducial jet parameters  $\Gamma = 300$ ,  $\gamma_m = 100$  and  $p = 2.2$ , the EIC spectrum peaks at  $\nu_p \sim 10 \text{ GeV}$ . The EIC spectrum below  $\nu_p$  is  $\nu L_\nu \propto \nu^2$  and  $\propto \nu^{-0.5}$  above  $\nu_p$ ; pair production softens the spectrum at high energies (above the threshold for  $e^\pm$  production). In *Case (III)*, significant EIC emission also comes from electrons accelerated by external shocks, where we use  $\epsilon_e = 0.1$  as the fraction of internal energy shared by hot electrons in the shocked regions.

In *Case (I)*, using binary separations  $10^{14} - 10^{16} \text{ cm}$ , we get EIC luminosities of  $10^{47} - 10^{50} \text{ erg/s}$  (the effect of pair production on high energy photon luminosity is included in this and all calculations below), peaking at separation  $10^{15} \text{ cm}$ . In *Case (II)*, soft photons originally from the progenitor star are scattered first by the electrons in the stellar wind and again by the jet. Using a W-R-star mass loss rate  $10^{-5} M_\odot/\text{yr}$  and wind velocity  $10^8 \text{ cm/s}$ , we get an EIC luminosity of  $10^{48} \text{ erg/s}$ . In *Case (III)*, we assume that stars in the cluster create a uniform EPF. Electrons in the jet are accelerated by both internal dissipation (ID) and external shocks. We include both the reverse shock and forward shock. Using stellar number density  $10^4 \text{ pc}^{-3}$  and cluster radius  $1 \text{ pc}$ , we get EIC luminosities of  $10^{49} \text{ erg/s}$  from ID, and  $10^{49} \text{ erg/s}$  from external reverse shock and  $10^{46} \text{ erg/s}$  from external forward shock. The EIC emission from ID lasts for  $t_{obs} \simeq T_j \sim 10 \text{ s}$ , but that from external shocks lasts longer, approximately  $200 \text{ s}$  from reverse shock and  $2 \times 10^4 \text{ s}$  from forward shock.

We note that EIC emission from ID relies on the assumption that electrons are hot at the right radius  $r_{eff}$ :  $\sim d$  (the binary separation, *Case I*),  $\sim r_{tr}$  ( $\sim 3 \times 10^{14} \text{ cm}$ , the radius where the jet becomes transparent, *Case II*) and  $10^{16} \text{ cm } r_{max,16}$  (the maximum radius electrons stay hot, *Case III*). In addition, EIC emission from external shocks strongly depends on the dynamical evolution of the jet.

Generally, from a GRB at redshift  $z = 1$ , a photon fluence of  $10^{-7} - 10^{-4} \text{ cm}^{-2}$  at  $1 - 100 \text{ GeV}$  is expected. Future observations (by e.g. *Fermi* LAT, HAWC and CTA) can put constraints on: (1) the existence of such EPFs as described in this paper and hence on the nature of GRB progenitors; (2) the radius where the jet internal dissipation process accelerates electrons.

## ACKNOWLEDGMENTS

The authors thank M. Milosavljević, P. Crumley, R. Santana, R. Hernández for helpful discussions. G.F.S. acknowledges support through his Chaire d'Excellence Université

Sorbonne Paris Cité and the financial support of the Uni-  
vEarthS Labex program at Université Sorbonne Paris Cité  
(ANR-10-LABX-0023 and ANR-11-IDEX-0005-02).

**REFERENCES**

Abdo, A. A., Ackermann, M., Ajello, M., et al. 2010, *ApJ*, 720, 435  
 Abeysekara, A. U., Aguilar, J. A., Aguilar, S., et al. 2012, *Astroparticle Physics*, 35, 641  
 Abeysekara, A. U., Alfaro, R., Alvarez, C., et al. 2015, *ApJ*, 800, 78  
 Acciari, V. A., Aliu, E., Arlen, T., et al. 2011, *ApJ*, 743, 62  
 Ackermann, M., Ajello, M., Asano, K., et al. 2013, *ApJS*, 209, 11  
 Ackermann, M., Ajello, M., Asano, K., et al. 2014, *Science*, 343, 42  
 Aharonian, F. A., & Atoyan, A. M. 1981, *Ap&SS*, 79, 321  
 Aharonian, F., Akhperjanian, A. G., Barres de Almeida, U., et al. 2009, *A&A*, 495, 505  
 Albert, J., Aliu, E., Anderhub, H., et al. 2007, *ApJ*, 667, 358  
 Atwood, W. B., Abdo, A. A., Ackermann, M., et al. 2009, *ApJ*, 697, 1071  
 Band, D., Matteson, J., Ford, L., et al. 1993, *ApJ*, 413, 281  
 Bernlöhr, K., Barnacka, A., Becherini, Y., et al. 2013, *Astroparticle Physics*, 43, 171  
 Blandford, R. D., & McKee, C. F. 1976, *Physics of Fluids*, 19, 1130  
 Blumenthal, G. R., & Gould, R. J. 1970, *Reviews of Modern Physics*, 42, 237  
 Bromm, V. 2013, *Reports on Progress in Physics*, 76, 112901  
 Casanova, S., Dingus, B. L., & Zhang, B. 2007, *ApJ*, 656, 306  
 Chevalier, R. A., Li, Z.-Y., & Fransson, C. 2004, *ApJ*, 606, 369  
 Crowther, P. A. 2007, *ARA&A*, 45, 177  
 Dermer, C. D., & Schlickeiser, R. 1993, *ApJ*, 416, 458  
 Espinoza, P., Selman, F. J., & Melnick, J. 2009, *A&A*, 501, 563  
 Fan, Y.-Z., Piran, T., Narayan, R., & Wei, D.-M. 2008, *MNRAS*, 384, 1483  
 Foley, R. J., Smith, N., Ganeshalingam, M., et al. 2007, *ApJL*, 657, L105  
 Fruchter, A. S., Levan, A. J., Strolger, L., et al. 2006, *Nature*, 441, 463  
 Galama, T. J., Vreeswijk, P. M., van Paradijs, J., et al. 1998, *Nature*, 395, 670  
 Ghisellini, G., Lazzati, D., Celotti, A., & Rees, M. J. 2000, *MNRAS*, 316, L45  
 Giannios, D. 2008, *A&A*, 488, L55  
 Gilmore, R., & Ramirez-Ruiz, E. 2010, *ApJ*, 721, 709  
 Gilmore, R. C., Somerville, R. S., Primack, J. R., & Domínguez, A. 2012, *MNRAS*, 422, 3189  
 Gruber, D., Goldstein, A., Weller von Ahlefeld, V., et al. 2014, *ApJS*, 211, 12  
 Guetta, D., & Granot, J. 2003, *MNRAS*, 340, 115

Hammer, F., Flores, H., Schaerer, D., et al. 2006, *A&A*, 454, 103  
 Heger, A., & Woosley, S. E. 2002, *ApJ*, 567, 532  
 Hjorth, J., Sollerman, J., Møller, P., et al. 2003, *Nature*, 423, 847  
 Inoue, S., Granot, J., O'Brien, P. T., et al. 2013, *Astroparticle Physics*, 43, 252  
 Kiewe, M., Gal-Yam, A., Arcavi, I., et al. 2012, *ApJ*, 744, 10  
 Kobayashi, S. 2000, *ApJ*, 545, 807  
 Kobulnicky, H. A., Kiminki, D. C., Lundquist, M. J., et al. 2014, *arXiv:1406.6655*  
 Kumar, P., & Smoot, G. F. 2014, *MNRAS*, 445, 528  
 Kumar, P., & Zhang, B. 2015, *Physics Reports*, 561, 1  
 Lada, C. J., & Lada, E. A. 2003, *ARA&A*, 41, 57  
 Langer, N. 2012, *ARA&A*, 50, 107  
 Lazzati, D., Ghisellini, G., Celotti, A., & Rees, M. J. 2000, *ApJL*, 529, L17  
 MacFadyen, A. I., & Woosley, S. E. 1999, *ApJ*, 524, 262  
 MacFadyen, A. I., Woosley, S. E., & Heger, A. 2001, *ApJ*, 550, 410  
 Madau, P., & Phinney, E. S. 1996, *ApJ*, 456, 124  
 Mason, B. D., Hartkopf, W. I., Gies, D. R., Henry, T. J., & Helsel, J. W. 2009, *AJ*, 137, 3358  
 Massey, P., & Hunter, D. A. 1998, *ApJ*, 493, 180  
 Matzner, C. D. 2003, *MNRAS*, 345, 575  
 Mészáros, P. 2006, *Reports on Progress in Physics*, 69, 2259  
 Mimica, P., & Giannios, D. 2011, *MNRAS*, 418, 583  
 Panaitescu, A., & Kumar, P. 2001, *ApJL*, 560, L49  
 Piran, T. 2004, *Reviews of Modern Physics*, 76, 1143  
 Portegies Zwart, S. F., McMillan, S. L. W., & Gieles, M. 2010, *ARA&A*, 48, 431  
 Ramirez-Ruiz, E. 2004, *MNRAS*, 349, L38  
 Sana, H., de Mink, S. E., de Koter, A., et al. 2012, *Science*, 337, 444  
 Smartt, S. J. 2009, *ARA&A*, 47, 63  
 Stacy, A., & Bromm, V. 2013, *MNRAS*, 433, 1094  
 Suwa, Y., & Ioka, K. 2011, *ApJ*, 726, 107  
 Uhm, Z. L. 2011, *ApJ*, 733, 86  
 Wanderman, D., & Piran, T. 2010, *MNRAS*, 406, 1944  
 Woosley, S. E. 1993, *ApJ*, 405, 273  
 Woosley, S. E., & Bloom, J. S. 2006, *ARA&A*, 44, 507  
 Zinnecker, H., & Yorke, H. W. 2007, *ARA&A*, 45, 481

**APPENDIX A:**

There are two potential pair-production channels that could absorb the high energy (10 – 100 GeV) the EIC photons. (1) In the lab frame, the EPF (~ 10 eV) will interact with ~ 100 GeV photons. We show below that this channel is usually not important. (2) In the jet comoving frame, the GRB prompt emission (~ 1 keV) will interact with ~ 1 GeV photons (~ 100 GeV in the lab frame). We consider this channel in detail, following Madau & Phinney (1996); Gilmore & Ramirez-Ruiz (2010), and this channel is included in our numerical calculation (Section 2).

**A1 Absorption by EPF Itself**

The only concern here is for photons of energy  $\geq 100$  GeV. The optical depth of pair production is

$$\tau_{\gamma\gamma} \simeq n_\gamma \sigma l \quad (\text{A1})$$

where  $l$  is the path length of the high energy  $\gamma$ -ray through the EPF,  $n_\gamma$  is the number density of field photons near the energy of maximum cross section, and  $\sigma \simeq 0.1\sigma_T$  is the approximate cross section.

In the *Binary Case*, most scatterings happen at radius  $r \sim d$ , so we have

$$\tau_{\gamma\gamma}^{(1)} \simeq \frac{L_b}{4\pi(d^2 + d^2)\epsilon_0 c} \left(1 - \frac{\sqrt{2}}{2}\right) \sigma d = 1.6 \times 10^{-2} \frac{L_{b,39}}{d_{14\epsilon_0,1}} \quad (\text{A2})$$

In the *Wind Case*, most scatterings happen at radius  $r \sim r_{tr}$  (see Eq.21 and 26), so we have

$$\tau_{\gamma\gamma}^{(2)} \simeq \frac{L_b \tau_{wind}(r_{tr})}{4\pi r_{tr}^2 \epsilon_0 c} \sigma r_{tr} = 2 \times 10^{-6} \frac{\Gamma_{2.5} L_{b,39} \dot{M}_{-5}}{E_{j,54} \eta_{KN} \epsilon_{0,1} v_8} \quad (\text{A3})$$

In the *Star Cluster Case*, EIC photons need to penetrate the whole cluster that has radius  $R = 1 pc R_{pc}$ , so we have

$$\tau_{\gamma\gamma}^{(3)} \simeq \frac{n_* L_b R}{\epsilon_0 c} \sigma R = 4.5 \times 10^{-1} \frac{n_{*,4} L_{b,39} R_{pc}^2}{\epsilon_{0,1}} \quad (\text{A4})$$

These are upper limits, since some EPF photons are either offset from the maximum cross section energy or at energy lower than the threshold. Anyway, the absorption is only important in *Binary Case* when  $d \lesssim 10^{12}$  cm and in *Star Cluster Case* when  $R \gtrsim 1$  pc. Under these conditions, there will be a spectral cut off at  $> \sim 100$  GeV. The absorption is not important in *Wind Case*. A more detailed calculation is given by Gilmore & Ramirez-Ruiz (2010).

**A2 Absorption by GRB Prompt Emission**

In the jet comoving frame, a high energy EIC photon of frequency  $\nu'$  is surrounded by low energy photons (frequency  $\nu'_i$ ), which can be described by the so-called Band function (Band et al. 1993). We simplify the Band function as a broken powerlaw of indexes  $\alpha_1$  and  $\alpha_2$ , below and above the break frequency  $\nu_b$ . From the prompt emission bolometric isotropic luminosity  $L_\gamma$ , and the radius  $r$  where the low energy photons are produced, we get the comoving-frame specific number density

$$n'_{\nu'_i}(r) = \frac{L_\gamma}{4\pi r^2 c h \nu_b^2} \left( \frac{1}{\alpha_1 + 2} - \frac{1}{\alpha_2 + 2} \right)^{-1} \begin{cases} (\nu'_i/\nu_b)^{\alpha_1} & \text{if } \nu'_i < \nu_b \\ (\nu'_i/\nu_b)^{\alpha_2} & \text{if } \nu'_i > \nu_b \end{cases} \quad (\text{A5})$$

where  $\nu'_b = \nu_b/\Gamma$  is the break frequency in the comoving frame. The pair-production threshold is

$$h\nu'_{th} = \frac{2(m_e c^2)^2}{h\nu'(1 - \cos\theta'_i)} \quad (\text{A6})$$

where  $\theta'_i$  is the angle between high( $\nu'$ ) and low( $\nu'_i$ ) energy photons' momentum vectors. The cross section for pair production is (Madau & Phinney 1996)

$$\sigma_{\gamma\gamma}(\nu', \nu'_i, \theta'_i) = \frac{3\sigma_T}{16} (1 - q^2) \left[ (3 - q^4) \ln \frac{1+q}{1-q} + 2q(q^2 - 2) \right] \quad (\text{A7})$$

where  $q = \sqrt{1 - \nu'_{th}/\nu'_i}$ . Assuming that low energy photons are moving isotropically in the jet comoving frame, we get the mean free path

$$l_{\gamma\gamma}^{-1}(\nu', r) = \frac{1}{2} \int_{-1}^1 d(\cos\theta'_i) (1 - \cos\theta'_i) \int_{\nu'_{th}}^\infty d\nu'_i n'_{\nu'_i} \sigma_{\gamma\gamma} \quad (\text{A8})$$

Then the pair-production optical depth is the comoving dynamical timescale divided by the mean time interval between two collisions, i.e.

$$\tau_{\gamma\gamma}(\nu', r) = \frac{r}{\Gamma l_{\gamma\gamma}(\nu', r)} \quad (\text{A9})$$

Therefore, only a fraction  $e^{-\tau_{\gamma\gamma}}$  of the EIC photons in Eq.(13) can escape. A simple estimate of the pair-production optical depth is

$$\tau_{\gamma\gamma} \simeq 0.1\sigma_T \frac{L_\gamma/4}{4\pi r^2 c h \nu'_{th} \Gamma^2} \frac{r}{\Gamma} \simeq 0.65 \frac{L_{\gamma,52}(h\nu/10\text{GeV})}{r_{15}\Gamma_{2.5}^4} \quad (\text{A10})$$

where we assume 1/4 of all the prompt  $\gamma$ -rays contribute to the absorption of high energy photons. We can see: (1)  $\tau_{\gamma\gamma}$  is very sensitive to the bulk Lorentz factor (we have used  $\Gamma = 300\Gamma_{2.5}$ ); (2) most absorption happens at small radius ( $r_{15} \leq 1$ ) and high frequency ( $h\nu \geq 10$  GeV).